Western Graduate&PostdoctoralStudies

Western University
Scholarship@Western

Electronic Thesis and Dissertation Repository

9-28-2021 10:00 AM

Using Hyperspectral Near-Infrared Spectroscopy and Diffuse Correlation Spectroscopy to Monitor the Effects of Phenylephrine in the Microcirculation

Laura Mawdsley, *The University of Western Ontario*

Supervisor: Ellis, Christopher G., *The University of Western Ontario*
Joint Supervisor: Diop, Mamadou, *The University of Western Ontario*
A thesis submitted in partial fulfillment of the requirements for the Master of Science degree in Medical Biophysics
© Laura Mawdsley 2021

Follow this and additional works at: https://ir.lib.uwo.ca/etd

 Part of the Analytical, Diagnostic and Therapeutic Techniques and Equipment Commons

Recommended Citation

Mawdsley, Laura, "Using Hyperspectral Near-Infrared Spectroscopy and Diffuse Correlation Spectroscopy to Monitor the Effects of Phenylephrine in the Microcirculation" (2021). *Electronic Thesis and Dissertation Repository*. 8294.
https://ir.lib.uwo.ca/etd/8294

This Dissertation/Thesis is brought to you for free and open access by Scholarship@Western. It has been accepted for inclusion in Electronic Thesis and Dissertation Repository by an authorized administrator of Scholarship@Western. For more information, please contact wlswadmin@uwo.ca.

Abstract

The microcirculation is the site of oxygen exchange in the body, and little work has been done to determine if different microvascular beds respond similarly to a simultaneous vascular challenge. A hybrid microvascular monitoring device was developed that uses hyperspectral near-infrared spectroscopy and diffuse correlation spectroscopy to simultaneously monitor the brain and skeletal muscle. Experiments were conducted on Sprague Dawley rats (n=6, 156g±6.4g) to discern the effect that phenylephrine (0.1 mL bolus, 10 mg/kg) has on the mean arterial pressure (MAP), hemoglobin concentration, and blood flow in each microvasculature. Hemoglobin concentration increased by 2.1±0.2 mmol in the brain, and decreased by 2.5±1.0 mmol in skeletal muscle. Cerebral blood flow increased by 20.8±7.2% while muscular blood flow decreased by 7.5±1.5%. The response in the brain was dependent on the initial baseline MAP. This non-invasive method can be used to aid in clinical translation of findings in animal models.

Keywords

Microcirculation, Near-infrared Spectroscopy, Diffuse Correlation Spectroscopy, Cerebral, Musculoskeletal, Phenylephrine, Blood Flow, Hemoglobin.

Summary for Lay Audience

The microcirculation is the distal functioning unit of the cardiovascular system, where small blood vessels called capillaries are responsible for oxygen exchange. Red blood cells travel through capillaries and transport the protein responsible for carrying oxygen in the body, hemoglobin. The microcirculation regulates oxygen delivery, but the needs of the microcirculation changes from organ to organ; muscular blood flow can change nearly 100-fold, where cerebral blood flow must remain relatively constant.

Hemoglobin is a main light absorber in tissue, and we can take advantage of this light absorbing property to monitor changes in its characteristics non-invasively using light-based methods. This thesis accomplishes this by using two optical methods: hyperspectral near infrared spectroscopy (*h*-NIRS) and diffuse correlation spectroscopy (DCS). The *h*-NIRS device uses a white halogen lamp that was simultaneously directed at both the rat scalp to monitor the brain and the rat left hind limb to monitor the skeletal muscle. The DCS device uses a laser, which emits light at a single near-infrared wavelength, that was also simultaneously directed at both the brain and the skeletal muscle. Multiple injections of a vasoconstrictor, which constricts larger blood vessels like arteries and arterioles, were administered to increase blood pressure.

The purpose of this work was to develop a hybrid *h*-NIRS/DCS system that can simultaneously monitor the microcirculation in the brain and in skeletal muscle, and to demonstrate that this system can monitor changes in tissue dynamics. Comparing the results from the brain to those from skeletal muscle, we found that the response of the brain depended highly on the baseline blood pressure while the results for skeletal muscle do not. When blood pressure was low, there was an increase of blood to the brain and vice versa. This difference in response between the brain and skeletal muscle is likely due to strict regulation that occurs in the brain. This device could be used in diseases like diabetes and sepsis that have been shown to have microvascular deficits, as well as help bridge the gap between small animal disease models and what is seen in patients.

Co-Authorship Statement

A version of the second chapter titled “Using hyperspectral near infrared spectroscopy and diffuse correlation spectroscopy to monitor the microvascular effects of phenylephrine in vivo” was published as a conference proceeding by SPIE. Laura Mawdsley was the first author for this work, and the remaining co-authors are Ajay Rajaram, Lawrence C.M. Yip, Naomi Abayomi, Stephanie Milkovich, Keith St. Lawrence, Jeffrey J.L. Carson, Christopher G. Ellis and Mamadou Diop.

Laura Mawdsley was responsible for the study design, data collection, data analysis, and drafting the manuscript. Ajay Rajaram and Lawrence C.M. Yip adapted and built the hybrid *h*-NIRS/DCS system. Ajay Rajaram also supplied the in-house DCS data acquisition software. Naomi Abayomi adapted the first version of the DCS analysis code for the original one written by Mamadou Diop. Stephanie Milkovich assisted with the animal surgery required to perform the experiments. Keith St. Lawrence and Jeffery J.L. Carson assisted with the study concept. As co-supervisors, both Christopher G. Ellis and Mamadou Diop directed the study concept, design, data interpretation, and editing the manuscript. Mamadou Diop also finalized Naomi Abayomi’s DCS analysis MATLAB code. All authors reviewed and approved the manuscript prior to publication.

Acknowledgments

This thesis was truly a team effort, and would not have been possible without the encouragement and guidance from my entire support system.

First to my co-supervisor Dr. Chris Ellis, thank you for taking me in as an undergrad and shaping the scientist that I am today. I will always be in awe of your vast breadth of knowledge and your pure excitement about science. I would not have accepted a spot in this program without your continued excitement about the possibilities of our work and your confidence in my skills, even when I didn't see it myself.

To my co-supervisor Dr. Mamadou Diop, I can't describe how much I appreciated your enthusiasm about this project, your open-door policy, and your seemingly endless patience when I mixed up the reference and background spectrum for the 20th time. Thank you for dedicating countless hours out of your busy schedule to mentor me, as I would not be the scientist I am today without your wisdom, and example.

I will always be indebted to you both for the skills I have developed during my time here, and I am privileged to have learned from you both.

I would like to acknowledge the final person on my advisory committee, Dr. John McGuire. Your thoughts and suggestions shaped this project, and were priceless to the success of this research. Furthermore, the invaluable help from Steph Milkovich truly made this project possible. I am so thankful you took the time to teach me such a complex protocol, and that you were always around when I needed a second hand tying off the art line. To all my lab mates, both past and present, you helped shape this degree into more than just research. Thank you for your ideas when I was feeling lost, your cheers when things went well, and your friendship along the way. Thank you to Ajay Rajaram and Lawrence Yip, who were instrumental in the beginning stages of this project as we designed and built the optics system. Thank you to David Cohen, as this thesis would've taken much longer to write without our hours and hours on Zoom. I couldn't have asked for a better proctor!

Lastly, thank you to my friends and family for your endless love and support. You were all willing at a moment's notice to provide a listening ear, or a well-timed distraction. To my parents specifically, thank you for letting me come home and thank you for graciously listening while I complained about not living in the mountains.

Table of Contents

List of Tables

List of Figures

List of Abbreviations

BFI	Blood Flow Index
CAR	Cerebral Autoregulation
CBF	Cerebral Blood Flow
DCS	Diffuse Correlation Spectroscopy
h-NIRS	Hyperspectral Near Infrared Spectroscopy
Hb	Deoxygenated Hemoglobin
HbO	Oxygenated Hemoglobin
HbT	Total Hemoglobin
MAP	Mean Arterial Pressure
NIR	Near Infrared
NIRS	Near Infrared Spectroscopy
RBC	Red Blood Cell/Erythrocyte

Chapter 1

1 Introduction

This introductory chapter will present the motivation for conducting the research presented in this thesis. This section will focus on providing a background on skeletal muscle and brain regulation mechanisms, the mechanism of action of phenylephrine, and an overview of the theories and technologies of the light-based methods used herein. The aims and objectives of the research are presented in the final subsection.

1.1 Microcirculation

Capillary networks are distal functioning units of the cardiovascular system, as oxygen delivery and carbon dioxide removal occur at the capillary level (Fagrell, 1997), (Segal, 2005). Red blood cells (RBCs) are specialized to transport respiratory gases (Daly, 2013) via the oxygen carrying protein, hemoglobin.

The microcirculation is often depicted as a tree-like structure of arteries, capillaries, and veins, structurally arranged to optimize oxygen transport. Arteries and arterioles deliver oxygenated blood to tissues, then venules and veins drain low oxygen blood from capillaries and return it to the heart and lungs. The main determinant of geometric flow resistance is the arteriolar tree and the available surface area for oxygen exchange is the structure of capillary networks.

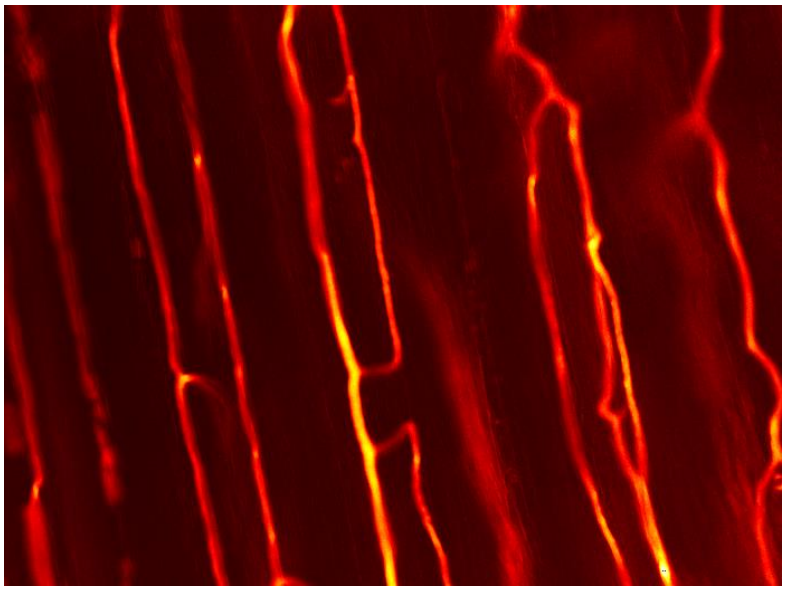

Figure 1.1: Image derived from a video of the microcirculation illustrating the layout of capillaries. The brighter and more yellow hued the pixel, the more red blood cells that passed though the capillary during the collection time.

1.1.1 Blood Flow Regulation

A functional microcirculation must exert dynamic control over tissue oxygenation, despite the short diffusion distance of oxygen from the blood into the surrounding tissue (Ellis, 2005), (Weibel, 1984). Capillary red blood cell hemodynamics determine convective oxygen delivery of flowing blood (Lo, 2003), which can be denoted as capillary perfusion within microvascular networks (Mendelson, 2021). The microvasculature must be responsive to changes in metabolic demand and adjust flow accordingly.

The microvascular network, including arterioles, capillaries and venules, must act as a coordinated vasomotor system that controls distribution of blood flow into tissues (Segal, 2005). Arteries and arterioles regulate the flow of oxygen-rich blood into capillaries. Several control systems work in conjunction to accomplish this, including neural impulses, circulating hormone factors, local myogenic responses, and retrograde conducted vascular signaling (Segal, 2005), (Clifford, 2011). When it comes to supporting metabolic demand, the oxygen requirements of tissue must have a close relationship to oxygen supply.

Skeletal muscle is the largest organ by mass, and the largest capillary bed in the body (Poole, 2013). It also has the widest range in metabolic requirements, as muscular blood flow can change nearly 100-fold and therefore it needs robust regulation methods for dealing with the large swings in oxygen demand (Thomas, 2004), (Murrant, 2015), (Poole, 2013). Regulation in skeletal muscle is a complex system, as even microvascular architecture is not static (Ellsworth, 2016). Regulatory control is based on pressure (myogenic control) and flow rate (shear stress) that control arteriolar vessel diameter, while neural, humoral, and metabolic regulatory systems adjust systemic and local microvascular pressure and flow. In capillaries, where the diameter often mirrors the diameter of RBCs, the assumption that blood acts as a uniform liquid no longer holds true. As seen in (Ellis, 1992) RBCs travel single file though capillaries, interspersed with plasma gaps. Many theories have been suggested that would explain the mechanisms of increased blood flow to skeletal muscle, including oxygen sensitivity in arterioles (Pittman, 1973), the release of nitrite from arterioles (Gladwin, 2004), and two RBC-dependent mechanisms. RBCs are the "best" choice of oxygen sensor since they carry oxygen, which has led to a few proposed methods of RBC-based regulation. The first concerns the release of S-nitrothiol - the deoxygenation of hemoglobin has been shown to release S- nitrothiol (Stamler, 1997). It is thought to cause vasodilation in arterioles, however this method of oxygen regulation has been rebutted (Patel, 1999), (Gladwin, 2003). The more likely theory concerns the release of ATP from RBCs (Ellsworth, 1995), (Ellsworth, 2016). The RBC releases ATP to induce an increase in oxygen supply to specific regions of tissue. The amount of ATP released from RBCs directly relates to the oxygen needs of the tissue bed (Jagger, 2001). This model has been supported by various theoretical papers and models (Ellis, 2010), (Ellsworth, 2009), (Goldman, 2012) as well as in vivo evidence (Ghonaim, 2021), (Sové, 2021).

Comparatively, the brain does not have such dramatic swings in oxygen requirements. Cerebral blood flow (CBF) is an important biomarker of brain health and function and CBF impairment is a direct cause of clinical conditions such as ischemic stroke (Durduran, 2014). Much like any other tissue bed, the cerebral vasculature is a highly complex, interconnected network of vessels. Blood is supplied to the brain though 4 main vessels,

but after this stage the vasculature mimics the skeletal muscle structure described above: blood passes into arterioles, then capillaries, and drains through venules into veins. Due to the high metabolic demand in the brain, it requires continuous CBF. CBF is controlled by a process called cerebral auto regulation (CAR). CAR is the intrinsic ability of the cerebral vasculature to maintain consistent blood flow despite changes or fluctuations in cerebral perfusion pressure (Lassen, 1959) and it typically works when the mean arterial pressure is between 60 and 150 mmHg (Paulson, 1990). CAR is especially important as the brain has no way to store oxygen within the organ, therefore any disruption in supply would quickly result in tissue oxygenation depletion and metabolic stress (Boas, 2011). CAR closely controls CBF by modulating vascular resistance (Paulson, 1990), as autoregulation is achieved almost entirely through the control of vessel radius (Payne, 2016). Nearly all accepted models of autoregulation revolve around feedback via arterial compliance. Four mechanisms are proposed for autoregulation: myogenic, neurogenic, metabolic, and endothelial (Armstead, 2016). In severely challenging circumstances, normal regulation methods may be overwhelmed. Instead, neurogenic and sympathetic control may take over (ter Laan, 2013). Much like skeletal muscle regulation, CAR is not completely understood as there is no consensus on which CAR assessment or monitoring approach should be considered the gold standard (Liu, 2020). However, it is generally regulated through changes in arteriolar diameter which drive changes in vascular resistance (Budohoski, 2013), (Fog, 1938), (Kontos, 1978), (Symon, 1973). In response to variation in arterial blood pressure, and therefore cerebral perfusion pressure, cerebral vascular resistance will adapt to return CBF to acceptable levels. Cerebral perfusion pressure is not the only variable, as vascular smooth muscle cells can also modify cerebral vascular resistance in response to a carbon dioxide stimulus (Hoiland, 2019). In addition, recent work looking at regional differences in cerebral vascular resistance concluded that assuming the effect on the middle cerebral artery could be applied across the brain is likely incorrect (Ainslie, 2009), (Skow, 2013). Therefore, the gold standard for measurement needs to have an approach that improves on the regional accuracy.

1.1.2 Phenylephrine

The microvasculature responds to changes in metabolic demand caused by a variety of endogenous and exogenous compounds. Phenylephrine is a commonly used drug that, when given intravenously, is an effective vasopressor in a variety of clinical settings (Ertmer, 2009). It binds to adrenergic receptors and induces contraction of vascular smooth muscle cells. This vasoconstriction can last up to twenty minutes in humans, with the maximum blood pressure occurring one-minute post injection (Ertmer, 2009), (Dancker, 2018). Phenylephrine is routinely used in cardiac surgery, to increase mean arterial pressure and systemic vascular resistance without affecting cardiac output.

Despite the well-known effects of phenylephrine on mean arterial pressure, its effects on the microcirculation are unclear; phenylephrine has been shown to either significantly decrease microvascular oxygen saturation and blood flow (Maier, 2009), (Poterman, 2015), (Van Leishout, 2008), (Meng, 2011) or cause no change (Strandgaard, 2008), (Hengstmann, 1982), (Faraci, 1990) in various microvascular beds and patient populations. One location of interest is skeletal muscle; as mentioned previously microvascular blood flow in skeletal muscle is controlled by a variety of regulating sympathetic mechanisms (Ogoh, 2011). Phenylephrine disrupts the sympathetic nervous control of skeletal muscle by binding to α-adrenergic receptors causing vasoconstriction (Christensen, 2017). This vasoconstriction in skeletal muscle is responsible for the increase in blood pressure seen with phenylephrine administration. This causes an increase in flow in most organs. An exception to this may be the brain, which is what makes the brain an additional region of interest. Cerebral autoregulation plays a central role in regulating the cerebral microcirculation, which is done by tightly regulating cerebral blood flow by modulating processes such as vascular resistance (Paulson, 1990). Studies have shown that resistance in large arteries and microvascular vessels are both affected by circulating vasoconstrictors (Faraci, 1990), and it has been further shown that cerebral autoregulation can be impaired by phenylephrine (Meng, 2011), (Hudlicka, 2011). Thus, there is a need to determine the effects of this commonly used drug on cerebral and skeletal muscle microcirculation.

1.2 Measuring Blood Flow

Non-invasive methods for measuring microvascular blood flow include single-photon emission computed tomography (SPECT), positron emission tomography (PET), MRI with contrast agents, Doppler ultrasound, and arterial spin labeling (ASL) MRI. However, standard radiological methodologies (MRI, PET, CT) are obviously not practical for continuous monitoring and often require a tracer or a contrast agent. Transcranial Doppler is limited to observations of larger blood vessels and not the arterioles and capillaries (Li, 2021).

Two alternative options for non-invasive microvascular monitoring are Near Infrared Spectroscopy and Diffuse Correlation Spectroscopy. A more detailed description of each modality is provided in sections 1.3 and 1.4, respectively.

1.3 Near-Infrared Spectroscopy

Near Infrared Spectroscopy (NIRS) is a non-invasive, light-based method that illuminates tissue with near infrared light to measure the concentration of chromophores. NIRS typically uses light in the 650-1000nm range to penetrate more deeply into tissue than visible light (Jobsis, 1997), (Fantini, 2018). NIRS measurements of hemoglobin concentration changes in the brain through the intact skull are feasible because of weak absorption of NIR light by hemoglobin and the other tissue chromophores, and relatively small tissue scattering as first demonstrated by (Jobsis, 1977). In the NIR window, there are only a few endogenous chromophores that have distinct absorption features and a large enough concentration to be easily measured with NIRS. The most physiologically significant of these is hemoglobin, whose molar extinction coefficient depends on oxygen saturation (SO_2) of the hemoglobin molecule, and is wavelength dependent (Kewin, 2018).

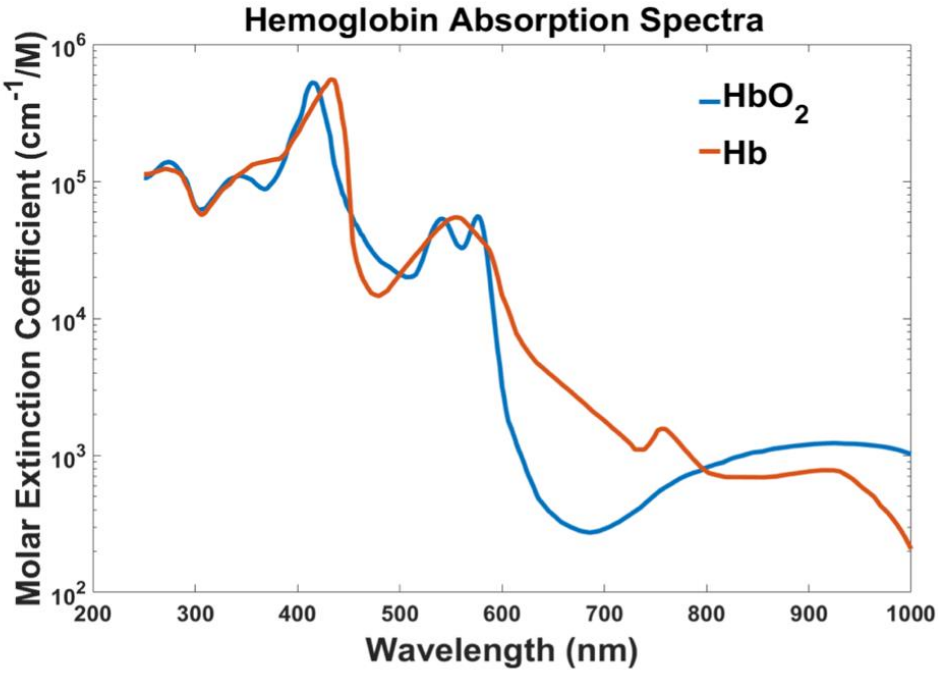

Figure 1.2: Absorption spectra of both oxygenated hemoglobin (blue) and deoxygenated hemoglobin (red) in the near infrared (NIR) range (650-1000nm).

As mentioned previously, hemoglobin is the oxygen carrying protein in blood and is therefore an ideal candidate for monitoring tissue oxygen saturation. The spectral features of hemoglobin allow for the concentration of each of its states (oxygenated and deoxygenated) to be continuously monitored by quantifying the amount of NIR light absorption at several wavelengths within the spectral range.

1.3.1 Principles of NIRS

Modelling of light propagation through tissue has led to the ability to estimate physiological parameters such as blood flow and tissue oxygenation, due in large part to the quantification of the absorption and scattering coefficients using analytical models such as the diffusion approximation to the radiative transfer equation (Boas, 1997), (Yodh, 1995), (Delpy, 1997).

The device used in this thesis is based on continuous-wave, hyperspectral NIRS (*h*-NIRS) technology. There are two other NIRS technologies, namely frequency-domain and time-resolved but their discussion is outside the scope of this thesis. Continuous-wave is the simplest and most widely used type of NIRS, where light of constant intensity is used to probe the tissue of interest. Most commercial NIRS devices use just a few (2-3); Hb and HbO are quantified by measuring light attenuation at these wavelengths, then a model is applied to convert the measurements into hemoglobin concentrations (Strangman, 2003). In contrast, hyperspectral NIRS measures light absorption at dozens of wavelengths to allow for more accurate estimation of the concentration of Hb and HbO (Kewin, 2019); the hyperspectral NIRS device used in this thesis cover the wavelengths of 650-1000nm. The approach used in this thesis was adopted from (Diop, 2015). Light propagation in the probed tissue was modeled using a solution to the diffusion approximation for a semi-infinite homogenous medium, which characterizes the light in terms of the absorption coefficient (μ_a) and the reduced scattering coefficient (μ_s') (Fantini, 1994). The wavelength-dependent reduced scattering coefficient can be expressed as (Jacques, 2013):

$$\mu_s' = A\left(\frac{\lambda}{800}\right)^{-a} \tag{1.1}$$

where A is the μ_s' value at 800nm, and a is the scattering power. The absorption coefficient is given by its relationship with the concentration of oxygenated hemoglobin (HbO), deoxygenated hemoglobin (Hb), and water:

$$\mu_a(\lambda) = [HbO] \cdot \varepsilon_{HbO}(\lambda) + [Hb] \cdot \varepsilon_{Hb}(\lambda) + WF \cdot \varepsilon_{H_2O}(\lambda) \tag{1.2}$$

where $\varepsilon(\lambda)$ represents the extinction coefficient of Hb and HbO, and *WF* is the tissue water fraction. While not explicitly provided in this work, the estimated concentrations of deoxygenated and oxygenated hemoglobin can be used to compute tissue oxygenation (Diop, 2014).

Total hemoglobin (HbT) is the sum of Hb and HbO, and is a clinically relevant measure of blood oxygen transport capacity (Hayashi, 2020). It is determined by:

$$HbT = Hb + HbO \tag{1.3}$$

1.3.2 NIRS in Tissue

The light that reaches larger vessels such as arteries and veins is almost completely absorbed due to the higher amount of hemoglobin that travels through these vessels; as such, NIRS light effectively interrogates the microcirculation (De Backer, 2012), (Taylor, 1996), (Boushel, 2000). A non-invasive oxygen sensor would have significant clinical utility for assessing tissue injury and disease that give rise to impaired oxygen delivery and/or utilization, and would be important for following tissue response to therapy (Boas, 2011). Other advantages of NIRS include its portability, ability to accomplish non-invasive monitoring, and its relative low cost. The main organs that are interrogated with NIRS are skeletal muscle and the brain (Barstow, 2019), (Ferrari, 2012), (Hilty, 2019) but monitoring of other organs have also been investigated. Notably, NIRS has been used to study a variety of muscle groups in humans as outlined nicely in various review articles (Hamaoka, 2007), (Ferrari, 2011), (Jones, 2017), (Barstow, 2019). Further, since the brain exhibits a high rate of oxygen metabolism (Edvinsson, 1993), it is not surprising that majority of NIRS studies have been focused on the brain (Durduran, 2014). NIRS was first used in the human brain by (Brazy, 1985) and has been used successfully applied many times since (Arora, 2013), (Milej, 2020), (Abdalmalak, 2020), (Kewin, 2019), (Lange, 2019), (Diop, 2012), (Diop, 2010), (Elliot, 2010). Limitations of NIRS include signal contamination by skull and/or adipose tissue, the unknown effect of myoglobin on the signal, and the effect of blood volume changes on optical pathlength (Ferrari, 2004).

1.4 Diffuse Correlation Spectroscopy

Diffuse correlation spectroscopy (DCS) is an optical technique that utilizes NIR light to directly and non-invasively measure local microvascular blood flow (Durduran, 2010). DCS has a lot of the same advantages as NIRS (i.e., non-invasive, cost effective) but with the added benefit of measuring blood flow without the need for a tracer or contrast agent (Busch, 2018), (Boas, 1995), (Buckley, 2014). DCS can monitor blood flow with high temporal resolution by measuring temporal intensity fluctuations in coherent light, which are characterized by generating an autocorrelation function (Guoqiang, 2005), (Boas, 1995). Higher flow rates lead to a loss of coherence which translates into a decrease in autocorrelation. This relationship allows for the measurement of blood flow via a blood flow index (BFI) (Diop, 2011), (Selb, 2014), (Boas, 2016), (Boas, 1995). DCS measurements are often converted into blood flow index (BFI), which is a relative blood flow measurement obtained by computing the changes in the diffusion coefficient relative to a baseline period (Li, 2021). Although BFI doesn't have traditional or absolute blood flow units, it is directly proportional to tissue blood flow (Diop, 2011), (Li, 2015), (He, 2018).

Summarized from (Verdecchia, 2016), the theory behind DCS is outlined below. NIR photons undergo multiple scattering interactions with RBCs in tissue. The electric fields of the photons that emerge from the tissue interfere at the surface of the skin either constructively or destructively to produce bright and dark spots (speckle pattern). Moving RBCs cause fluctuations in the speckle pattern; when the RBCs move faster (slower), these fluctuations change quicker (slower), causing a decrease (increase) in temporal coherence. This measure of the degree of phase correlation can be used to assess changes in tissue perfusion by computing an autocorrelation function from the measured intensity fluctuations.

Furthermore, in the 1990's, there was a discrepancy between two well-known theories that describe energy transfer: radiative transport and correlation transport (Ackerson, 1992). Radiative transport assumes that energy is conserved, while correlative transport does not; however, this difference can be explained by scattering. Applying this difference to a

highly scattering, low absorbing media lead to the correlation diffusion equation (Boas, 1995). This equation can be solved to generate a model that characterizes RBC motion in the microcirculation, as RBC motion is the predominant cause of the loss of coherence (Ninck, 2010). In this thesis, since the thickness of the rat skin and skull (when relevant) is relatively thin, we assumed that the tissue under investigation was a semi-infinite homogenous medium.

Due to the reliance of DCS analysis on coherence, the quality of the light source is crucial; a single wavelength, long-coherence laser is needed. The long coherence length is important to ensure the light is in phase after traveling a relatively large distance through the tissue. This ensures any decorrelation is due to interactions with scatterers, and not from the source itself. Further, a single mode or a few mode detection fibre and a NIR light-sensitive single photon counting module are required. A single mode detection fibre has a small diameter to ensure that only one or a few speckles are sampled, and the single photon counting module allows for high signal to noise ratio.

1.4.1 DCS in Tissue

DCS was first used in tissue in the early 2000s and has been growing in popularity ever since (Buckley, 2014), (Mazumder, 2021). DCS has been extensively validated through comparisons with various techniques, including Doppler ultrasound (Buckley, 2009), (Roche-Labarbe, 2010), Xenon CT (Kim, 2010), MRI (Milej, 2019) and others (Zhou, 2009), (Durduran, 2004), (Yu, 2007), (Diop, 2011). DCS has significant advantages in measuring BFI: the relatively large interrogation depth (Ubbink, 1993), (Chen, 1997) sensitivity to the microcirculation, and lack of radiation exposure. The main limitation of DCS is the possibility for signal contamination from extracerebral tissues, causing an underestimation of CBF (Verdecchia, 2016).

The application of DCS to neuromonitoring is gaining traction, with many studies done in piglets (Zhou, 2009), (Verdecchia, 2013) and neonates (Rajaram, 2020), (Roche-Labarbe, 2010) thanks to their thin skull thickness. The use of DCS in muscle focuses heavily on exercise induced effects, such as handgrip exercises (Rosenberry, 2019), cycling

(Quaresima, 2019), and flexion (Shang, 2010), (Yu, 2005). An understudied field of research is using DCS to quantify the outcomes of drugs with vasoconstricting/dilating effects on the heterogeneity of skeletal muscle.

1.5 NIRS and DCS Used Together

Individually, NIRS and DCS have demonstrated their ability to accurately detect disease- or bolus-induced physiological changes in tissues. However, using NIRS and DCS together has the potential to provide more robust measures. For example, HbT and blood flow are proving to be better indicators of tissue status compared to SO_2 alone (Meek, 1999), (Grant, 2009), and even better when combined with CBF to estimate oxygen consumption (Yoxall, 1998), (Roche-Labarbe, 2010), (Durduran, 2010). It has been shown that SO_2 alone is not robust enough (Weiss, 2005), and NIRS can only be used to directly measure CBF if a tracer is used (Durduran, 2014), (Diop, 2010). However, combining hemoglobin concentration, oxygen saturation, and blood flow has been shown to be a robust indicator of tissue viability (Christensen, 2017).

The largest roadblock in combining these two systems is ensuring that no cross-talk occurs between the two systems, as they both operate in the same wavelength range. A popular solution is using a multiplexing approach based on mechanical shutters to ensure only one system is transmitting and receiving light at a time (Rajaram, 2018), (Mawdsley, 2021). While this solution does not allow for a true simultaneous collection, shutter cycles can be relatively short (~3 seconds) to ensure adequate temporal resolution.

First introduced in rats to collect blood flow and oxygen saturation data (Cheung, 2001), hybrid *h*-NIRS/DCS systems have proven beneficial for continuous *in vivo* monitoring in piglets (Verdecchia, 2013), humans (Rajaram, 2020), (Rajaram, 2018), and in multiple microvascular beds in rats (Mawdsley, 2021). Incorporation of *h*-NIRS/DCS into the same instrumentation creates a new opportunity to make comprehensive, all-optical

measurements of cerebral hemodynamics and cerebral oxygen metabolism (Durduran, 2014).

1.6 Research Objectives

The increasing wide-spread use of hybrid NIRS/DCS systems opens doors for a variety of important insights into normal physiology and pathological conditions. An overlooked advantage of these systems is the possibility to not only simultaneously monitor the vasculature using two techniques, but also the monitoring multiple microvascular beds simultaneously. Determining the effect of an intervention in one organ (i.e., the brain) is important, but determining the effect on two+ organs simultaneously can provide additional insight into how the body works as a whole, and how the responses of the different microvascular beds may differ.

This work focused on developing a hybrid *h*-NIRS/DCS system that can achieve near-simultaneous monitoring of two microvascular beds in live animals: the brain and skeletal muscle. This is the first report of simultaneous monitoring of the cerebral and muscular microcirculation, and the first to concurrently monitor the effects of phenylephrine on blood pressure, the brain, and skeletal muscle. This work lays the ground for future studies, such as monitoring the time course of microvascular response in diseases like sepsis and diabetes, and the effects of commonly used drugs on multiple organs.

The specific objectives of this work were as follows:

1. Develop a hybrid *h*-NIRS/DCS system for use in small animals (rats specifically) that can simultaneously monitor the microcirculation in the brain and in skeletal muscle.
2. Demonstrate that the system can monitor changes in tissue hemodynamics by inducing a vascular challenge. This was provided by injection of a vasoconstrictor – phenylephrine – and subsequent monitoring.

1.7 References

1. Fagrell, B. and Intaglietta, M., “Microcirculation: its significance in clinical and molecular medicine,” J Intern Med 241(5), 349-362 (1997).
2. Segal, S.S., “Regulation of bood flow in the microcirculation,” Microcirculation 12(1), 33 – 45 (2005).
3. Daly, S. M., “'Go with the flow’: A review of methods and advancements in blood flow imaging,” J Biophotonics 6(3) , 217-255 (2012).
4. Ellis, C. G., Jagger, J. and Sharpe, M., “The microcirculation as a functional system,” Crit Care 9(Suppl 4), S3 - S8 (2005).
5. Weibel, E., “The pathway for oxygen,” Harvard University Press, Cambridge, MA (1984).
6. Lo, A. F., Fuglevand, A.J, and Secomb, T.W., “Oxygen delivery to skeletal muscle fibers: effects of microvascular unit structure and control mechanisms,” Am J Physiol Heart Circ Physiol 285(3), H955-H963 (2003).
7. Mendelson, A.A. et al., “The capillary fascicle in skeletal muscle: structural and functional physiology of RBC distribution in capillary networks,” J Physiol 599(8), 2149-2168 (2021).
8. Clifford, P.S., “Local control of blood flow,” Adv Physiol Educ 35(1), 5 – 15 (2011).
9. Poole, D.C. et al., “Skeletal muscle capillary function: Contemporary observations and novel hypotheses,” Exp Physiol 98(12), 1645 – 1658 (2013).
10. Thomas, G. S. and Segal, S.S., “Neural control of muscle blood flow during exercise” J Appl Physiol 97(2), 731-738 (2004).
11. Murrant, C.L. and Sarelius, I.H. “Local control of blood flow during active hyperaemia: what kinds of integration are important?,” J Physiol 593(21), 4699–4711 (2015).
12. Ellsworth, M.L., Ellis, C.G. and Sprague, R.S., “Role of erythrocyte-released ATP in the regulation of microvascular oxygen supply in skeletal muscle,” Acta Physiol (Oxf) 216(3), 265 – 276 (2016).
13. Ellis, C.G. et al., “Application of image analysis for evaluation of red blood cell dynamics in capillaries,” Microvascular Research 44(2), 214-225 (1992).
14. Pitman, R.N. and Duling, B.R., “Oxygen sensitivity of vascular smooth muscle: I. *In vitro* studies,” Microvasc Res 6(2), 202-211 (1973).

15. Gladwin, M.T. and Schechter, A.N., “NO contest: nitrite versus S-nitrosohemoglobin,” Circ Res 94(7), 851-855 (2004).
16. Stamler, J.S. et al., “Blood flow regulation by S-nitroshemoglobin in the physiological oxygen gradient,” Science (276(5321), 2034-2037 (1997)
17. Patel, R.P. et al., “Biochemical characterization of human S-nitrosohemoglobin effects on oxygen binding and transnitrosation,” Journal of Biological Chemistry 274(22), 15487-15482 (1999).
18. Gladwin, M.T. et al., “Nitric oxide’s reactions with hemoglobin: a view through the SNO-storm,” Nature Medicine 9(5), 496-500 (2003).
19. Ellsworth, M.L. et al., “The erythrocyte as a regulator of vascular tone,” Am J Physiol 269(6 pt 2), H2155-H2161 (1995).
20. Jagger, J.E. et al., “Role of erythrocyte in regulating local O_2 delivery mediated by hemoglobin oxygenation,” Am J Physiol Heart Circ Physiol 280(6), H2833-H2839 (2001).
21. Ellis, C.G. et al., “Defects in oxygen supply to skeletal muscle of prediabetic ZDF rats,” Am J Physiol Heart Circ Physiol 298(6), H1661 - H1670 (2010).
22. Ellsworth, M.L. et al., “Erythrocytes: Oxygen sensors and modulators of vascular tone in regions of low PO_2,” Physiology (Bethesda) 24, 107-116 (2009).
23. Goldman, D. et al., “Toward a multiscale description of microvascular flow regulation: O_2-dependent release of ATP from human erythrocytes and the distribution of ATP in capillary networks,” Front Physiol 3, 246 (2012).
24. Ghonaim, N.W. et al., “Evidence for role of capillaries in regulation of skeletal muscle in oxygen supply,” Microcirculation e12699 (2021).
25. Sové, R.J. et al., “Localized oxygen exchange platform for intravital video microscopy investigations of microvascular oxygen regulation,” Front Physiol 12, 654928 (2021).
26. Durduran, T. and Yodh, A.G., “Diffuse correlation spectroscopy for non-invasive, micro-vascular cerebral blood flow measurement,” NeuroImage 85(1), 61-63 (2014).
27. Lassen, N.A., “Cerebral blood flow and oxygen consumption in man,” Physiol Rev 39(2), 183-238 (1959).

28. Paulson, O.B., Strandgaard, S. and Edvinsson, L., “Cerebral autoregulation,” Cerebrovasc Brain Metab Rev 2(2), 161-192 (1990).
29. Boas, D.A. and Franceschini, M.A., “Haemoglobin oxygen saturation as a biomarker: the problem and a solution,” Philos Trans A Math Phys Eng Sci 369(1955), 4407-4424 (2011).
30. Payne, S., “Cerebral autoregulation: control of blood flow in the brain,” Springer Publishing, Oxford UK (2016).
31. Armstead, W.M., “Cerebral blood flow autoregulation and dysautoregulation,” Anesthesiol Clin 34(3), 465-477 (2016).
32. ter Laan, M. et al., “Sympathetic regulation of cerebral blood flow in humans: a review,” British Journal of Anesthesiology 111(3), 361-367 (2013).
33. Liu, X. et al., “Assessment of cerebral autoregulation indices – a modelling perspective,” Scientific Reports 10, 9600 (2020).
34. Budohoski, K.P. et al., “Clinical relevance of cerebral autoregulation following subarachnoid haemorrhage,” Nature Reviews Neurology 9(3), 152-163 (2013).
35. Fog, M., “The relationship between the blood pressure and the tonic regulation of the pial arteries,” J Neurol Psychiatry 1(3), 187-197 (1938).
36. Kontos, H.A. et al., “Responses of cerebral arteries and arterioles to acute hypotension and hypertension,” Am J Physiol 234(4), H371-H383 (1978).
37. Symon, L., Held, K. and Dorsch, N.W., “A study of regional autoregulation in the cerebral circulation to increased perfusion pressure in normocapnia and hypercapnia,” Stroke 4(2), 139-147 (1973).
38. Hoiland, R.L., Fisher, J.A. and Ainslie, P.N., “Regulation of the cerebral circulation by arterial carbon dioxide,” Compr Physiol 9(3), 1101-1154 (2019).
39. Ainslie, P.N. and Duffin, J., “Integration of cerebrovascular CO2 reactivity and chemoreflex control of breathing: mechanisms of regulation, measurement, and interpretation,” Am J Physiol Regul Integr Comp Physiol 296(5), R1473-R1495 (2009).
40. Skow, R.J. et al., “Differential cerebrovascular CO_2 reactivity in anterior and posterior cerebral circulations,” Respir Physiol Neurobiol 189(1), 76-86 (2013).

41. Ertmer, C., Morelli, A. and Westphal, M., "The role of phenylephrine in perioperative medicine," Yearbook of Intensive Care and Emergency Medicine 1, 483-491 (2009).
42. Dancker, C., et al., "Effects of dobutamine, dopamine, phenylephrine and noradrenaline on systemic haemodynamics and intestinal perfusion in isoflurane anaesthetised horses," Equine Veterinary Journal 50(1), 104-110 (2018).
43. Maier, S., et al., "Effects of phenylephrine on the sublingual microcirculation during cardiopulmonary bypass," Br J Anaesth 102(4), 485-491 (2009).
44. Poterman, M., et al., "Differential effects of phenylephrine and norepinephrine on peripheral tissue oxygenation during general anaesthesia: a randomized control trial," Eur J Anaesth 32(8), 571-580 (2015).
45. Van Leishout, J. J. and Secher, N. H., "Point:Counterpoint: Sympathetic activity does/does not influence cerebral blood flow," J Appl Physiol 105(4), 1364-1366 (2008).
46. Meng, L., et al., "Effect of phenylephrine and ephedrine bolus treatment on cerebral oxygenation in anaesthetized patients," Br J Anaesth 107(2), 209-217 (2011).
47. Strandgaard, S. and Sigurdsson, S.T., "Counterpoint: Sympathetic activity does/does not influence cerebral blood flow," J Appl Physiol 105(4), 1366-1367 (2008).
48. Hengstmann, J.H. and Goronzy, J., "Pharmacokinetics of ^{3}H-phenylephrine in man," European Journal of Clinical Pharmacology 21, 335-341 (1982).
49. Faraci, F.M. and Heistad, D.D., "Regulation of large cerebral arteries and cerebral microvascular pressure," Circ Res 66(1), 8-17 (1990).
50. Ogoh, S., et al., "The effect of phenylephrine on arterial and venous cerebral blood flow in healthy subjects," Clin Physiol Funct Imaging 31(6), 445-451 (2011).
51. Christensen, L.K., et al., "Hemodynamic responses and plasma phenylephrine concentrations associated with intranasal phenylephrine in children," Paediatr Anaesth 27(7), 768-773 (2017).
52. Hudlicka, O., "Microcirculation in skeletal muscle," Muscles Ligaments Tendons J 1(1), 3-11 (2011).
53. Li, 2021
54. Jobsis, F. F., "Noninvasive, infrared monitoring of cerebral and myocardial oxygen sufficiency and circulatory parameters," Science 198(4323), 1264-1267 (1977).

55. Fantini, S., Frederick, B. and Sassaroli, A., “Perspective: Prospects of non-invasive sensing of the human brain with diffuse optical imaging,” APL Photonics 3, 110901 (2018).
56. Kewin, M., "Validation of a hyperspectral NIRS method for measuring tissue oxygen saturation," Electronic Thesis and Dissertation Repository, 5770 (2018).
57. Boas, D. and Yodh, A.G., “Scattering and imaging with diffusing temporal field correlations,” Physical Review Letters 75(9), 1855-1858 (1997)
58. Yodh, A. and Chance, B., “Spectroscopy and imaging with diffusing light,” Physics Today 48(3), 34-40 (1995).
59. Delpy, D.T. and Cope M., “Quantification in tissue near-infrared spectroscopy,” Philos Trans R Soc Lond B Biol Sci 352(1354), 649-659 (1997).
60. Strangman, G., Franceschini, M.A. and Boas, D.A., “Factors affecting the accuracy of near-infrared spectroscopy concentration calculations for focal changes in oxygenation parameters,” NeuroImage 18(4), 865-879 (2003).
61. Kewin, M. et al., “Evaluation of hyperspectral NIRS for quantitative measurements of tissue oxygenation saturation by comparison to time-resolved NIRS,” Biomed Opt Express 10(9), 4789-4802 (2019).
62. Diop, M., Kishimoto, J., Toronov, V., Lee, D. C. S. and St. Lawrence, K., “Development of a combined broadband near-infrared and diffusion correlation system for monitoring cerebral blood flow and oxidative metabolism in preterm infants,” Biomedical Optics Express 6(10), 3907-3918 (2015).
63. Fantini, S., Franceschini, M.A. and Gratton, E., “Semi-infinite-geometry boundary problem for light migration in highly scattering media: a frequency-domain study in the diffusion approximation,” J. Opt Soc Am B 11(10), 2128 (1994).
64. Jacques, S.L., “Optical properties of biological tissues: a review,” Phys. Med. Biol. 58(11), R37–R61 (2013).
65. Diop, M., Wright, E., Toronov, V., Lee, T. and St. Lawrence, K., “Improved light collection and wavelet de-noising enable quantification of cerebral blood flow and oxygen metabolism by a low-cost, off-the-shelf spectrometer” J of Biomedical Optics 19(5), 057007 (2014).

66. Hayashi, K., et al. “Influence of measurement principle on total hemoglobin value,” BMC Anesthesiology 20, 81 (2020).
67. De Backer, D., Donadello, K. and Orbegozo Cortes, D., “Monitoring the microcirculation,” Journal of Clinical Monitoring and Computing 26(5), 361-366 (2012).
68. Taylor, D.E. and Simonson, S.G., “Use of near-infrared spectroscopy to monitor tissue oxygenation,” New Horiz 4(4), 420-425 (1996).
69. Boushel, R. and Piantadosi, C.A., “Near-infrared spectroscopy for monitoring muscle oxygenation,” Acta Physiol Scand 168(4), 615-622 (2000).
70. Barstow, T.J., “Understanding near infrared spectroscopy and its application to skeletal muscle research” J Appl Physiol 126(5), 1360–1376 (2019).
71. Ferrari, M. and Quaresima, V., “Near infrared brain and muscle oximetry: From the discovery to current applications,” J Near Infrared Spectrosc 20 (1), 1–14 (2012).
72. Hilty, M.P. et al., “MicroTools enables automated quantification of capillary density and red blood cell velocity in handheld vital microscopy,” Commun Biol 2, 217 (2019).
73. Hamaoka, T. et al., “Near-infrared spectroscopy/imaging for monitoring muscle oxygenation and oxidative metabolism in healthy and diseases humans,” J Biomed Optics 12(6), 062105 (2007).
74. Ferrari, M., Muthalib, M. and Quaresima, V., “The use of near-infrared spectroscopy in understanding skeletal muscle physiology: recent developments,” Philos Trans A Math Phys Eng Sci 369, 4577-4590 (2011).
75. Jones, S. et al., “Recent developments in near-infrared spectroscopy (NIRS) for the assessment of local skeletal muscle microvascular function and capacity to utilize oxygen,” Artery Research 16, 25-33 (2017).
76. Edvinsson, L., MacKenzie, E.T. and McCulloch, J., “Cerebral blood flow and metabolism,” Raven Press, New York NY (1993).
77. Brazy, J. E. et al., “Noninvasive monitoring of cerebral oxygenation in preterm infants: preliminary observations,” Pediatrics 75(2), 1264-1267 (1985).
78. Arora, R. et al., “Preservation of the metabolic rate of oxygen in preterm infants during indomethacin therapy for closure of the ductus arteriosus,” Pediatric Research 73, 713-718 (2013).

79. Milej, D. et al., “Quantification of cerebral blood flow in adults by contrast-enhanced near-infrared spectroscopy: Validation against MRI,” J Cereb Blood Flow Metab 40(8), 1672-1684 (2020).
80. Abdalmalak, A. et al., “Assessing time-resolved fNIRS for brain-computer interface applications of mental communication,” Front Neurosci 14, 105 (2020).
81. Lange, P. and Tachtsidis, I., “Clinical brain monitoring with time domain NIRS: a review and future perspectives,” Appl Sci 9, 1612 (2019).
82. Diop, M. et al., “Towards non-invasive bedside monitoring of cerebral blood flow and oxygen metabolism in brain-injured patients with near-infrared spectroscopy,” Brain Injury – Pathogenesis, Monitoring, Recovery and Management, IntechOpen (2012).
83. Diop, M. et al., “Comparison of time-resolved and continuous wave near-infrared techniques for measuring cerebral blood flow in piglets,” J Biomed Opt 15(5), 057004 (2010).
84. Elliot, J.T. et al., “Quantitative measurement of cerebral blood flow in a juvenile porcine model by depth-resolved near-infrared spectroscopy,” J Biomed Opt 15(3), 037014 (2010).
85. Durduran, T. et al., “Diffuse optics for tissue monitoring and tomography,” Rep Prog Phys 73(3), 076701 (2010).
86. Busch, D.R. et al., “Detection of brain hypoxia based on non-invasive optical monitoring of cerebral blood flow with diffuse correlation spectroscopy,” Neurocritical Care 30, 72-80 (2018).
87. Buckley, E.M. et al., “Diffuse correlation spectroscopy for measurement of cerebral blood flow: future prospects,” Neurophotonics 1(1), 011009 (2014).
88. Guoqiang, Y. et al., “Near-infrared diffuse correlation spectroscopy for assessment of tissue blood flow,” in Handbook of Biomedical Optics, 195–216 (2005).
89. Boas, D. A., Campbell, L. E. and Yodh, A. G., “Scattering and imaging with diffusing temporal field correlations,” Phys Rev Lett 75(9), 1855-1858 (1995).
90. Diop, M. et al., “Calibration of diffuse correlation spectroscopy with a time-resolved near-infrared technique to yield *absolute* cerebral blood flow measurements,” Biomedical Optics Express 2(7), 2068-2081 (2011).

91. Selb, J. et al., “Sensitivity of near-infrared spectroscopy and diffuse correlation spectroscopy to brain hemodynamics: simulations and experimental findings during hypercapnia,” Neurophotonics 1(1), 015005 (2014).
92. Boas, D. A., Pitris, C. and Ramanujam, N., “Handbook of biomedical optics,” CRC Press, Boca Raton, FL (2016).
93. Li, Z. et al., “Calibration of diffuse correlation spectroscopy blood flow index with venous-occlusion diffuse optical spectroscopy in skeletal muscle,” Journal of Biomedical Optics 20(12), 125005 (2015).
94. He, L. et al., “Noninvasive continuous optical monitoring of absolute cerebral blood flow in critically ill adults,” Neurophotonics 5(4), 045006 (2018).
95. Verdecchia, K.J., "Digging deeper with diffuse correlation spectroscopy," Electronic Thesis and Dissertation Repository, 3930 (2016).
96. Ackerson, B.J. et al., “Correlation transfer - Application of radiative transfer solution methods to photon correlation problems,” Journal of Thermophysics and Heat Transfer 6(4), 577-588 (1992).
97. Ninck, M., Untenberger, M. and Gisler, T., “Diffusing-wave spectroscopy with dynamic contrast variation: disentangling the effects of blood flow and extravascular tissue shearing on signals from deep tissue,” Biomed Opt Exp 1(5), 1502-1513 (2010).
98. Mazumder, D. et al., “Optimization of time domain diffuse correlation spectroscopy parameters for measuring brain blood flow,” Neurophotonics 8(3), 035005 (2021).
99. Buckley, E.M. et al., “Cerebral hemodynamics in preterm infants during positional intervention measured with diffuse correlation spectroscopy and transcranial Doppler ultrasound,” Opt Express 17(15), 12571-12581 (2009)
100. Roche-Labarbe N. et al., “Noninvasive optical measures of CBV, StO(2), CBF index, and rCMRO(2) in human premature neonates' brains in the first six weeks of life,” Hum Brain Mapp 31(3), 341-352 (2010).
101. Kim, M.N. et al., “Noninvasive measurement of cerebral blood flow and blood oxygenation using near-infrared and diffuse correlation spectroscopies in critically brain-injured adults,” Neurocrit Care 12(2), 173-180 (2010).

102. Milej, D. et al., “Assessing Extracerebral Signal Contamination in Optical Measurements of Cerebral Blood Flow and Oxygenation,” Clinical and Preclinical Optical Diagnostics II, 11074_90 (2019).

103. Zhou, C., “Diffuse optical monitoring of hemodynamic changes in piglet brain with closed head injury,” J Biomed Opt 14(3), 034015 (2009).

104. Durduran, T. et al., “Diffuse optical measurement of blood flow, blood oxygenation, and metabolism in a human brain during sensorimotor cortex activation,” Opt Lett 29(15), 1766-1768 (2004).

105. Yu, G. et al., “Validation of diffuse correlation spectroscopy for muscle blood flow with concurrent arterial spin labeled perfusion MRI,” Opt Express 15(3), 1064-1075 (2007).

106. Ubbink, D.T. et al., “Skin microcirculation in diabetic and non-diabetic patients at different stages of lower limb ischaemia,” Eur J Vasc Surg 7(6), 659-6 (1993).

107. Chen, Z. et al., “Optical Doppler tomographic imaging of fluid flow velocity in highly scattering media,” Opt Lett 22(1), 64-66 (1997).

108. Verdecchia, K. et al., “Quantifying the cerebral metabolic rate of oxygen by combining diffuse correlation spectroscopy and time-resolved near-infrared spectroscopy,” J Biomed Opt 18(2), 027007 (2013).

109. Rajaram, A. et al., “Optical monitoring of cerebral perfusion and metabolism in adults during cardiac surgery with cardiopulmonary bypass,” Biomedical Optics Express 11(10), 5967-5981 (2020).

110. Rosenberry, R. et al., “Determinants of skeletal muscle oxygen consumption assessed by near-infrared diffuse correlation spectroscopy during incremental handgrip exercise,” J Appl Physiol 127(3), 698-706 (2019).

111. Quaresima, V. et al., “Diffuse correlation spectroscopy and frequency-domain near-infrared spectroscopy for measuring microvascular blood flow in dynamically exercising human muscles,” J Appl Physiol 127(5), 1328-1337 (2019).

112. Shang, Y. et al., “Effects of muscle fiber motion on diffuse correlation spectroscopy blood flow measurements during exercise,” Biomed Opt Express 1(2), 500-511 (2010).

113. Yu, G. et al., “Time-dependent blood flow and oxygenation in human skeletal muscles measured with non-invasive near-infrared diffuse optical spectroscopies,” J Biomed Opt 10(2), 024027 (2005).

114. Meek, J.H. et al., “Abnormal cerebral haemodynamics in perinatally asphyxiated neonates related to outcome,” Arch Dis Child Fetal Neonatal Ed 81(2), F110-F115 (1999).

115. Grant, P.E. et al., “Increased cerebral blood volume and oxygen consumption in neonatal brain injury,” J Cereb Blood Flow Metab 29(10), 1704-1713 (2009).

116. Yoxall, C.W. and Weindling, A.M., “Measurement of cerebral oxygen consumption in the human neonate using near infrared spectroscopy: cerebral oxygen consumption increases with advancing gestational age,” Pediatr Res 44(3), 283-290 (1998).

117. Weiss, M. et al., “Near-infrared spectroscopic cerebral oxygenation reading in neonates and infants is associated with central venous oxygen saturation,” Paediatr Anaesth 15(2), 102-109 (2005).

118. Cheung, C.C. et al., “In vivo cerebrovascular measurement combining diffuse near-infrared absorption and correlation spectroscopies,” Phys Med Biol 46(8), 2053-2065 (2001).

119. Rajaram, A. et al., “Perfusion and metabolic neuromonitoring during ventricular taps in infants with post-hemorrhagic ventricular dilation,” Brain Sci 10(7), 452 (2020).

120. Rajaram, A. et al., “Simultaneous monitoring of cerebral perfusion and cytochrome c oxidase by combining broadband near-infrared spectroscopy and diffuse correlation spectroscopy,” Biomedical topics Express 9(6), 2588-2603 (2018).

121. Mawdsley, L. et al., “Using hyperspectral near infrared spectroscopy and diffuse correlation spectroscopy to monitor the microvascular effects of phenylephrine in vivo," Proc. SPIE 11639, Optical Tomography and Spectroscopy of Tissue XIV, 116390Z (2021).

Chapter 2

2 In vivo monitoring of the effects of phenylephrine on the cerebral and musculoskeletal microvasculature with hyperspectral near-infrared spectroscopy and diffuse correlation spectroscopy

2.1 Introduction

The microcirculation is the distal functioning unit of the cardiovascular system, where blood moves through the vasculature via arterioles, capillaries and venules. A productive microcirculation must exert dynamic control over tissue oxygenation (Ellis, 2005), and for this to occur, the microvasculature must be responsive to changes in metabolic demand or challenges to oxygen supply and adjust blood flow accordingly (Segal, 2005).

The microvasculature responds to a variety of endogenous and exogenous compounds, such as hormones and medications. Phenylephrine is a commonly used drug that, when given intravenously, is an effective vasopressor in a variety of clinical settings (Ertmer, 2009). It binds to adrenergic receptors and induces contraction of vascular smooth muscle cells resulting in increased peripheral vascular resistance and blood pressure. This vasoconstriction can last up to twenty minutes in humans, with the maximum blood pressure occurring one-minute post injection (Ertmer, 2009), (Dancker, 2018). Phenylephrine is routinely used in cardiac surgery, to increase mean arterial pressure and systemic vascular resistance without affecting cardiac output, and often in sepsis-related arterial hypotension (Ertmer, 2009).

Despite the well-known effects of phenylephrine on mean arterial pressure, its effects on the microcirculation are inconsistent in organs such as the brain and peripheral tissue (Van Leishout, 2008), (Meng, 2011), (Strandgaard, 2008). Phenylephrine has been shown to either significantly decrease microvascular oxygen saturation and blood flow (Maier, 2009), (Poterman, 2015), (Van Leishout, 2008), (Meng, 2011) or cause no change (Strandgaard, 2008), (Hengstmann, 1982), (Faraci, 1990) in various microvascular beds and patient populations.

One location of interest is skeletal muscle; microvascular blood flow in skeletal muscle is controlled by a variety of regulating mechanisms, including nervous, hormonal, myogenic, and endothelial (Hudlicka, 2011). Phenylephrine affects the sympathetic nervous control of skeletal muscle by binding to α-adrenergic receptors causing vasoconstriction (Ogoh, 2011). An additional region of interest is the brain, as cerebral autoregulation plays a key role in regulating the cerebral microcirculation. This is done by tightly regulating cerebral blood flow in response to changes in arterial blood pressure by modulating processes such as vascular resistance (Paulson, 1990). Studies have shown that resistance in large arteries and the microvasculature are both affected by circulating vasoconstrictors (Faraci, 1990), and it has been further shown that cerebral autoregulation can be impaired by phenylephrine (Meng, 2011), (Christensen, 2017). However, there is a lack of data on the effect of phenylephrine on the cerebral microcirculation. Current literature implements a variety of monitoring methods with different temporal resolutions, preventing direct comparison of results between studies (Van Leishout, 2008), (Meng, 2011), (Strandgaard, 2008), (Strandgaard, 2008), (Hengstmann, 1982). Thus, there is a need to determine the effects of this commonly used drug on cerebral and skeletal muscle microcirculation.

Non-invasive monitoring of the microcirculation has become viable due to recent developments in optical technologies. One cost-effective method is hyperspectral near infrared spectroscopy (*h*-NIRS), which uses a broadband light source and a spectrometer to quantify changes in hemoglobin concentration and tissue oxygen saturation (Boas, 2011). Similarly, diffuse correlation spectroscopy (DCS) uses near infrared light to monitor changes in blood flow by analyzing temporal fluctuations of light scatter from red blood cells in the microvasculature. Combining these technologies to monitor hemoglobin concentration, oxygen saturation, and blood flow has been shown to be a robust indicator of tissue viability (Durduran, 2014). Hybrid *h*-NIRS/DCS systems have proven beneficial for continuous *in vivo* monitoring (Rajaram, 2020a), (Rajaram, 2020b), and provide a unique methodology for concurrent monitoring of hemodynamic parameters.

Using *h*-NIRS and DCS simultaneously to directly and continuously monitor hemodynamics in the brain and skeletal muscle microcirculation during a phenylephrine

injection will provide insight into the timing and impact of vasoconstriction on major microvasculature beds. The objective of the current study is to compare the effects of a timed phenylephrine bolus on the brain and skeletal muscle microvasculature.

2.2 Methods

2.2.1 Instrumentation

The monitoring device (Fig. 2.1A) was a hybrid *h*-NIRS/DCS system similar to the system reported by Rajaram (2018). The *h*-NIRS subsystem used a 20 W halogen light source (Ocean Insight HL-2000, FL, USA) whose output was simultaneously directed to the scalp and skeletal muscle via a bifurcated optical fibre bundle. Reflected light was collected with two fibre bundles (one on the scalp and one on the skeletal muscle, core = 400 μm, numerical aperture = 0.22, Thorlabs, NJ, USA) and guided back to two solenoid shutters (Digi-Key Electronics, MN, USA). A second set of identical fibre bundles guided light from the shutters' output to the two Ocean Insight spectrometers (MayaPro and QE65000, FL, USA); the MayaPro spectrometer monitored the brain and the QE65000 spectrometer collected measurements from the hind limb. The DCS subsystem used a 785 nm long coherence diode laser (CrystaLaser) with the output passing through a variable neutral density filter (NDC-100C-4M, Thorlabs, NJ, USA) into a bifurcated fibre bundle (core = 400 μm, numerical aperture = 0.22, Thorlabs, NJ, USA). Light then passed through a shutter into a second fibre bundle (core = 400 μm, numerical aperture = 0.22, Thorlabs, NJ, USA) that directed light into the target tissue (brain or skeletal muscle). A single mode fibre (core = 4.4 μm, numerical aperture = 0.13, Thorlabs, NJ, USA) collected the reflected light and brought it to a single photon counting module (SPCM, Laser Components, Germany). Fibre ends that collected light from tissue were fitted into a custom 3D printed probe holder (Fig. 1B) designed to be positioned on the left hind limb and the scalp. The source-detector distance was 10 mm for both the *h*-NIRS and DCS subsystems. Operation of both systems at the same time would result in cross-talk and compromised data, so shutters were used to ensure both light sources were not simultaneously illuminating the tissue. The control and timing of both subsystems originated from a TTL signal received from an in-house software built in LabView, which also controlled the 20 W light source

and four solenoid shutters – two between the DCS light source and the animal and two between the animal and the spectrometers (Fig. 2.1).

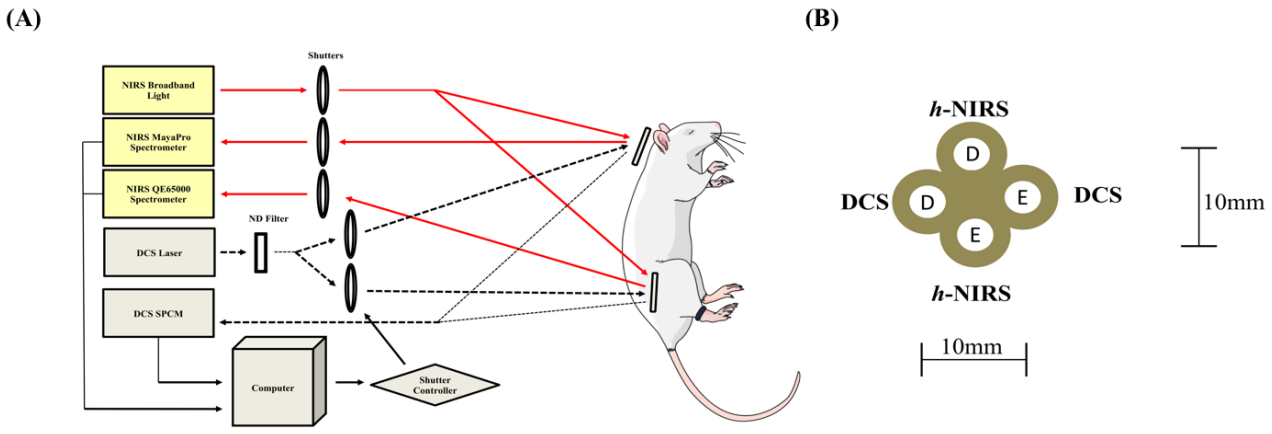

Figure 2.1: Schematic of the hybrid *h*-NIRS/DCS system (A) and probe holder (B). In (A), the red lines represent the *h*-NIRS signal path, and the black dashed lines represent the path of the DCS signal. In (B), the "E" represents the emission probes and the "D" represents the detection probes. Note that figures are not to scale.

2.2.2 Animal Protocol

2.2.2.1 Animal Model

This study was approved by Western University's Animal Care and Use Committee. Data were collected from male Sprague Dawley rats (n=6, 156±6.4g). Rats were anesthetized (pentobarbital, 65 mg/kg), then the carotid artery was cannulated to monitor blood pressure and the jugular vein was cannulated for the purpose of administering anesthetic and phenylephrine. A tracheotomy was performed to connect the rat to a ventilator to control breathing rate and ensure proper oxygen concentration in the administered gas mixture. 0.9% heparinized saline was used in the arterial flush line to prevent clotting and 0.9% saline was continuously infused through the venous line at a rate of 0.5 mL/hr. The core temperature of the animal was maintained at 37±0.5 °C using a rectal temperature probe and a heat mat. At this point, approximately 100 μL of arterial blood was collected and

analyzed using a portable point-of-care device (Vetscan iStat 1) to confirm healthy levels of blood gases (i.e., PO_2, PCO_2, pH) and lactate levels. Heart rate, temperature, and mean arterial pressure were monitored continuously throughout the experiment. An additional 100 μL of arterial blood was collected at the end of the experiment and analyzed with the same blood testing device.

2.2.2.2 Experimental Protocol

Once the surgery was completed, the fur on the top of the cranium and the left hind limb was removed with depilatory cream, and the background and reference spectra of the *h*-NIRS sub-system were acquired. One at a time, 6-8 injections were performed at 12-minute intervals: four to six boluses of a microvascular challenge, and 1-2 injections of a control (0.9% NaCl) solution. Measurements were obtained by recording baseline data for two minutes followed by a two-second injection of 0.1 mL of a phenylephrine-saline solution (10mg/kg of phenylephrine mixed with 0.9%NaCl solution (Yeh, 1999)) through the intravenous line. The line was then hand-flushed with 0.1mL of saline to ensure full and consistent dosing. DCS and *h*-NIRS measurements were acquired for 8 further minutes. Data were collected near-simultaneously thanks to the shutter multiplexing system. As shown in Figure 2.2, each modality collected data for 1 second, then all shutters were closed for 0.1 second, to account for any potential jitter, then the shutter for the next modality opened to collect data. The light source for the subsystem not in use was blocked by a shutter during the recording. The total length of a cycle was 3.3 seconds.

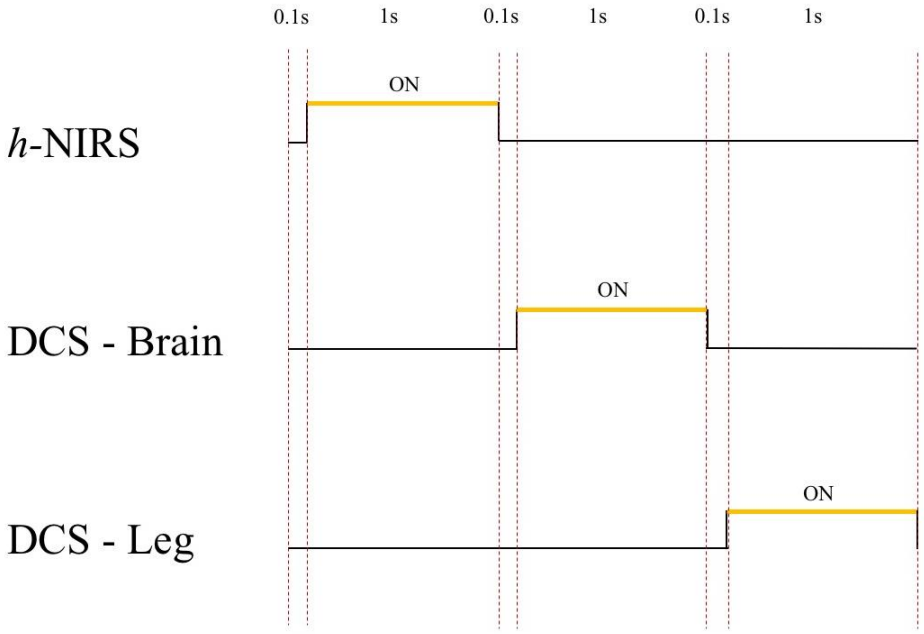

Figure 2.2: Schematic of the timing for the *h*-NIRS/DCS system. The system starts with 0.1sec of dark time, then opens the shutters for the *h*-NIRS halogen lamp and both spectrometers. After 1sec, the shutters for the halogen lamp and the spectrometers close and 0.1sec of dark time occurs. Next, the shutter for the brain DCS light source opens for 1 second, closes again for 0.1 second, and finally the shutter for the muscle DCS light source. The cycle repeats until the 10-minute of acquisition time is complete.

2.2.3 Data Processing

2.2.3.1 *h*-NIRS Data

For each challenge, the reflectance was calculated using the spectrum collected from the Maya and QE spectrometers using equation 1 (Diop, 2014):

$$R(\lambda) = \frac{spectrum_\lambda - background_\lambda}{reference_\lambda - background_\lambda} \quad (2.1)$$

where $R(\lambda)$ is the reflectance, $spectrum_\lambda$ is the spectrum measured from the animal, $background_\lambda$ is the background noise in spectrum from the spectrometer, and $reference_\lambda$ is the reference spectrum obtained from the light source.

Concentrations of chromophores (i.e., water, deoxygenated hemoglobin (Hb), and oxygenated hemoglobin (HbO)) were computed using the methods described by Diop (2015). Briefly, the first and second derivatives of R(λ) were fitted to the first and second derivatives of a solution to the diffusion approximation for a semi-homogenous medium (Fantini, 1994). The wavelength-dependent reduced scattering coefficient (μ_s') was modelled as:

$$\mu_s' = B\left(\frac{\lambda}{800}\right)^{-a} \tag{2.2}$$

where B represents the μ_s' value at λ = 800 nm, and a is the scattering power. The absorption coefficient (μ_a) was defined as:

$$\mu_a(\lambda) = [HbO] * \varepsilon_{HbO}(\lambda) + [Hb] * \varepsilon_{Hb}(\lambda) + [WF] * \varepsilon_{H_2O}(\lambda) \tag{2.3}$$

where ε(λ) represents the extinction coefficient of Hb and HbO, and *WF* is the tissue water fraction.

Concentrations of each chromophore were determined by using a two-step, multi-parameter fit for the first and second derivatives of the measured reflectance (Diop, 2015).

2.2.3.2 DCS Data

The blood flow index (BFI) was estimated using the methods described by Diop (2011). The dynamics of the moving light scatterers in the brain and skeletal muscle can be assessed by measuring the temporal dependence of the normalized intensity autocorrelation function which is related to the electric field autocorrelation function $G_1(\rho,\tau)$ by the Seigert relation (Cheung, 2001):

$$g_2(\rho,\tau) = 1 + \beta \frac{|G_1(\rho,\tau)|^2}{\{I(\rho,\tau)\}} \tag{2.4}$$

where β is the coherence factor, $G_1(\rho,\tau)$ is the solution to the diffusion equation and $\{I(\rho,\tau)\}$ represents the average detected intensity.

In highly scattering, low absorbing media the solution to the diffusion equation for large distances is $G_1(\rho,\tau)$. In this work, the data were analyzed using the solution to the diffusion equation for a semi-infinite homogenous medium (Diop, 2011):

$$G_1(\rho,\tau) = \frac{3\mu s'}{4\pi}\left(\frac{\exp(-k_D r_1)}{r_1} - \frac{\exp(-k_D r_2)}{r_2}\right) \quad (2.5)$$

The BFI was estimated by fitting the electric field autocorrelation curves obtained from the DCS measurements with a solution to the diffusion approximation for a semi-infinite homogenous medium (Fantini, 1994). The solution depends on the known source detector distance (10 mm), the tissue optical properties (μ_a, μ_s'), and the coherence factor. Each autocorrelation curve was fit over a range of correlation times (1-10μs) with blood flow index and the coherence factor as the fitting parameters, and μ_a and μ_s' set to their values for 785 nm, obtained from the *h*-NIRS analysis.

For both *h*-NIRS and DCS, data for all runs were averaged, and the standard error was calculated. Data are presented as a mean with standard error when appropriate. Analysis and statistical analysis were done with MATLAB_R2016b, using the Statistics tool box.

2.3 Results

Figure 2.3 shows data collected from all 3 data acquisition methods (blood pressure monitor, *h*-NIRS, and DCS) for a representative bolus. Figure 2.3A is illustrative of the systemic response to the bolus, as it is the rolling average of the mean arterial blood pressure (MAP) throughout the ten-minute capture. MAP increases by 38 mmHg immediately following the bolus, and slowly returns to baseline levels over the measurement period. Figures 2.3B and C show the percent change in cerebral (B) and

muscular (C) blood flow. Figures 2.3D and E show the absolute change in total hemoglobin in the brain and skeletal muscle, respectively.

As shown in Table 1, the cerebral blood flow increased post-bolus in some cases but decreased in others. However, by splitting the data based on the baseline MAP (using a 95 mmHg threshold), we realized that all CBFs measured at a baseline MAP lower than 95 mmHg increased post-bolus while all the CBFs acquired at a baseline MAP higher than 95 mmHg decreased. The mean arterial pressure across all boluses that increased, increased by 31±5.4 mmHg (Fig. 2.4A). The MAP across all boluses where CBF decreased, increased by 29±4.3 mmHg (Fig. 2.4B). The average baseline MAP for the increased CBF was 20 mmHg higher than the cases when CBF decreased (Fig. 2.4A). For the CBF increase dataset, total hemoglobin and cerebral blood flow also increased by 2.1±0.2 mmol, and 20.8±7.2%, respectively (Fig. 2.4C, 2.4E). Both total hemoglobin and CBF returned to a value slightly above baseline by the end of the 10-minute acquisition period. For the CBF decrease dataset, total hemoglobin decreased by 1.2±1.6 mmol immediately following the bolus and returned to baseline levels the end of the collection period (Fig. 2.4D); CBF decreased by 4.4±1.4% immediately following the bolus, then returned to baseline levels (Fig. 2.4F).

In contrast to the brain, the muscular blood flow response was consistent. Figure 2.5 displays the same data (mean arterial pressure, change in total hemoglobin, blood flow) for all boluses. MAP increased by 30±14.9 mmHg (Fig. 2.5A) in this dataset, with pressure returning to a value slightly above baseline by the end of the measurement period. Total hemoglobin and blood flow both initially decreased by 2.5±0.9 mmol and 7.6±1.4%, respectively (Fig. 2.5B, 2.5C) before returning to baseline levels. Figure 2.6 shows the relationship between the average baseline blood pressure and the maximum response in cerebral blood flow. As MAP increases, changes in the maximum CBF response decreases and even produces a decrease in CBF above 95 mmHg.

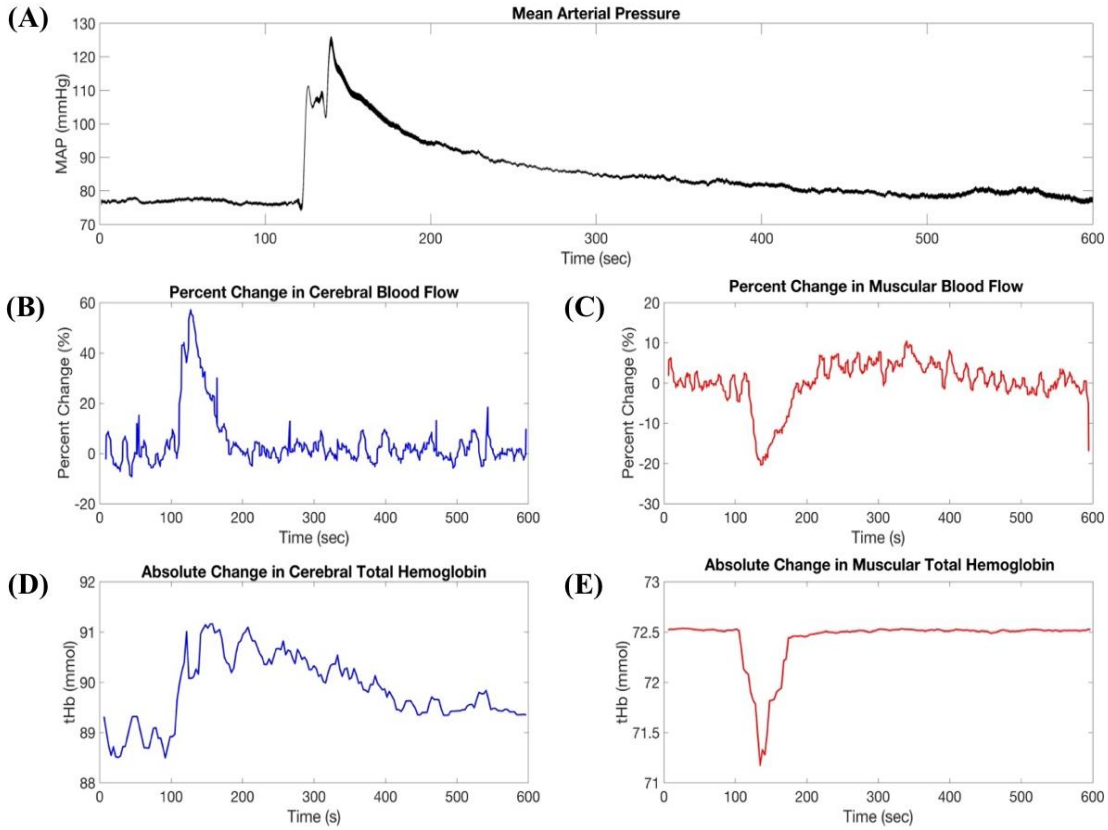

Figure 2.3: Representative data set demonstrating the typical systemic response to a phenylephrine bolus. The mean arterial pressure is shown in **(A)**, the percent change in cerebral blood flow and muscular blood flow in **(B)** and **(C)**, respectively, and the absolute change in total hemoglobin in the brain **(D)** and the muscle **(E)**.

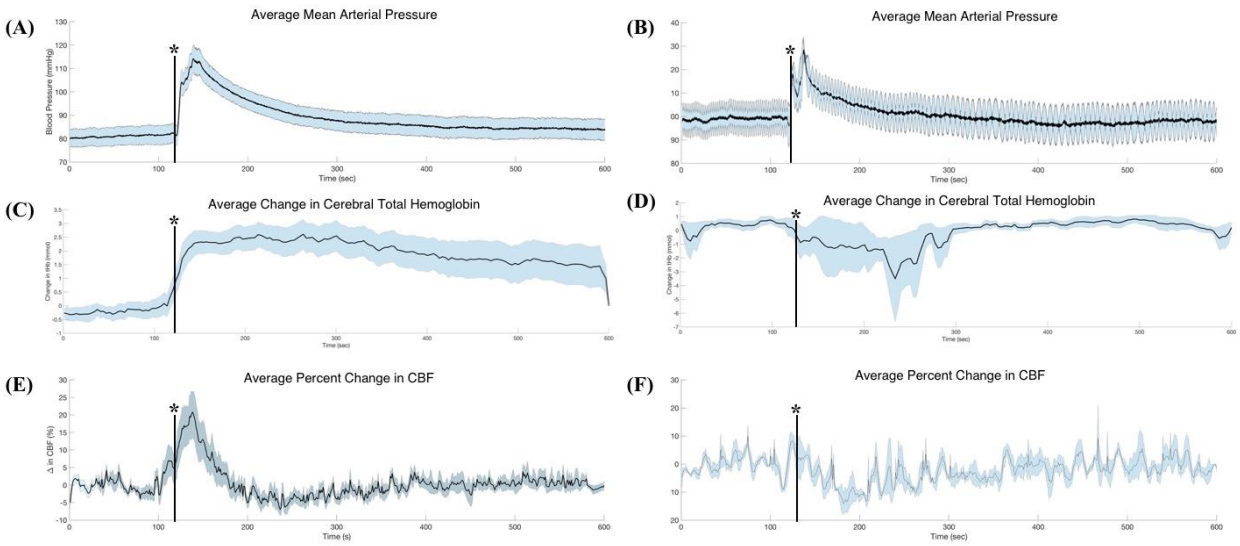

Figure 2.4: For all boluses that showed an increase in cerebral blood flow (CBF)(n=10), mean arterial pressure (MAP) is shown in (A), cerebral total hemoglobin is shown in (C), and percent change in CBF is shown in (E). For all boluses that showed a decrease in CBF (n=4), MAP is shown in (B), cerebral total hemoglobin in (D) and percent change in CBF in (F). The mean is shown in black, and the standard error is shown in blue shading. * represents when the phenylephrine bolus was administered.

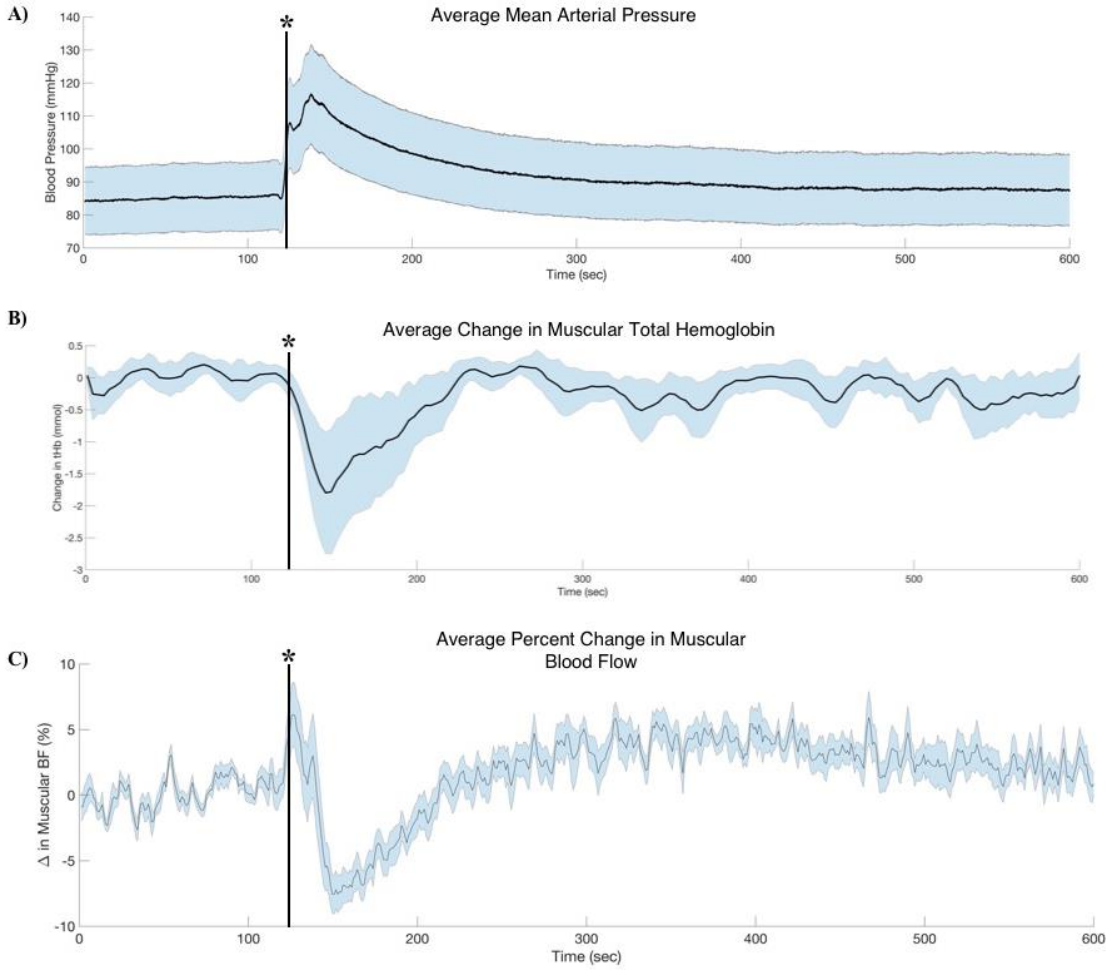

Figure 2.5: For all boluses in the skeletal muscle (n=31), the average MAP is shown in (A), the average change in total hemoglobin is shown in (B), and the average percent change in blood flow is shown in (C). * represents when the phenylephrine bolus was administered.

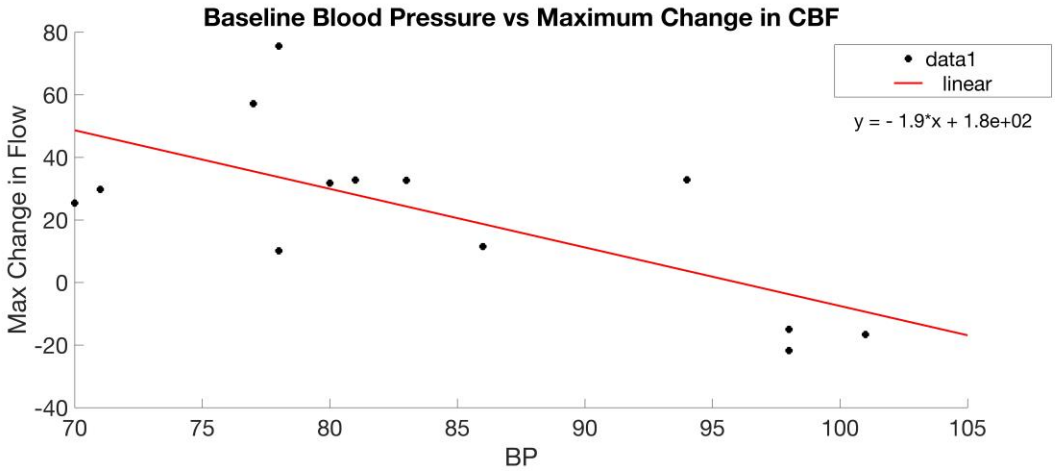

Figure 2.6: Relationship between the average baseline mean arterial blood pressure (pre-phenylephrine bolus) and the maximum percent change in cerebral blood flow.

Table 1: Blood pressure data and the trends associated with each phenylephrine bolus. "I" represents an increase at the time of injection, "D" represents a decrease at the time of injection, and an "N" represents a lack of data for that bolus.

Animal		Blood Pressure		HbT (*h*-NIRS)		Flow (DCS)	
Date	**Run**	**Baseline**	**Max Increase**	**Brain**	**Leg**	**Brain**	**Leg**
20200811	P1	71	50	I	D	I	D
20200811	P2	70	66	I	D	I	D
20200811	P3	78	55	I	D	I	D
20200811	P4	86	52	I	I	I	D
20200811	P5	92	45	I	D	D	D
20200818	P1	87	30	I	D	N	D
20200818	P2	95	31	I	D	N	D
20200818	P3	92	39	I	D	N	D
20200818	P4	87	37	I	D	N	D
20200818	P5	93	33	I	D	N	D
20200820	P1	105	30	D	D	N	D
20200820	P2	100	37	D	D	N	D
20200820	P3	110	40	D	D	N	D
20200820	P4	87	37	D	D	N	D
20200820	P5	91	32	D	D	N	D
20200820	P6	95	38	D	D	N	D
20200910	P1	105	28	D	D	N	D
20200910	P2	83	20	D	D	N	D
20200910	P3	92	31	N	D	N	D
20200910	P4	97	43	D	D	N	D
20200910	P5	101	36	I	D	N	D
20200910	P6	103	43	I	D	N	D
20200915	P1	81	35	I	D	I	D
20200915	P2	80	35	I	D	I	D
20200915	P3	83	57	I	D	I	D
20200915	P4	77	48	I	D	I	D
20200915	P5	78	56	D	D	I	D
20200917	P1	94	30	I	D	I	D
20200917	P2	98	32	I	D	D	D
20200917	P3	101	37	D	D	D	D
20200917	P4	98	36	D	D	D	D

2.4 Discussion

Using a hybrid *h*-NIRS/DCS system to directly and continuously monitor the cerebral and skeletal muscle microcirculation allows for non-invasive measurement of hemoglobin concentration and blood flow. Such technology can be used to determine the effect of phenylephrine across both microvascular beds. Both the MAP and the skeletal muscle response were expected; that is increased in MAP and flow, and decreased HbT. However, HbT and blood flow did not follow this same pattern in the brain, likely due to autoregulation. This is the first report of simultaneous use of *h*-NIRS and DCS to monitor the effects of phenylephrine on multiple microvascular beds in living animals.

The phenylephrine dosage was determined based on Yeh's 1999 experiment; this dosage caused a similar response to the desired effect in humans (Yeh, 1999). The effect of phenylephrine on mean arterial pressure (MAP) is well documented (Thiele, 2011), and is consistent with the findings of the current study. Baseline MAP stayed relatively constant, with an average post-bolus increase of 31 mmHg. The consistency of the MAP response is important to note; variability in microvascular responses was not due to fluctuating blood pressure between boluses. Unlike MAP, the microvascular beds responded differently to phenylephrine. Interestingly, HbT in the brain either showed a noticeable increase post bolus, or a gradual decrease post bolus. Further, the response in the "decrease cerebral flow" group had more variability.

Following the same trend as HbT, the cerebral blood flow either showed a noticeable increase post bolus, or a gradual decrease post bolus. As seen in Figure 2.6, larger than average baseline blood pressure was a precursor to a negative response. This pattern was not seen in the skeletal muscle flow data, implying that cerebral autoregulation may play a role in the observed CBF responses. It is important to note that these effects may be different in a sick or otherwise unhealthy animal, as phenylephrine is most commonly used to restore normal blood pressure and cerebral blood flow.

A benefit of near-simultaneous recording of two microvascular beds is that the response of each organ can be compared for the same bolus. Phenylephrine causes vasoconstriction in

arterioles in skeletal muscle, which is the driving force of the increase in MAP. As shown in this work, this increase causes a varying effect on the cerebral microcirculation, depending on the initial baseline MAP.

Cerebral autoregulation can be impaired by phenylephrine, which makes studying the effects of phenylephrine on the brain microvasculature all the more important. The phenylephrine bolus caused an increase in systemic blood pressure, but did not cause a consistent response in the brain. When the baseline MAP was lower than 95 mmHg, blood flow and HbT increased in the brain. In contrast, when the baseline MAP was higher than 95 mmHg, blood flow and HbT decreased. This data suggests that CAR works to increase flow to the brain at baseline pressures lower than 95 mmHg, but decrease flow at pressures higher than 95 mmHg. Since blood pressures above this point don't cause CAR to increase flow, the decrease seen may be due to the effects of phenylephrine on the large cerebral arterioles similar to what is seen in the muscle. This is in direct contrast to the muscle, which has no stringent protective effect like CAR to keep flow at a certain level. The regularity of the MAP and the skeletal muscle flow response is consistent with skeletal muscle being the driving force of the MAP increase, as muscle contraction and pressure are stable. Higher blood pressures seen in hypertension are associated with structural changes and dysfunctions that induce impaired cerebral autoregulation (Pires, 2013), (Shekar, 2017). This impairment is reflected in these data, where the response in higher blood pressures more closely mimics the response in skeletal muscle.

Our previous work (Mawdsley, 2021) has allowed the temporal resolution of the phenylephrine response in these two microvascular beds to be discerned. Those time courses showed that after an intravenous injection of phenylephrine, the microcirculation responds within three seconds. Additionally, hemoglobin concentration did not return to baseline levels during the collection window, suggesting that the collection window should be extended to determine whether the collection window was not long enough if in fact phenylephrine causes a lasting effect on hemoglobin and oxygen saturation levels. We extended the collection window from six to ten minutes, and the microvascular data mostly

returned to baseline in this time. As expected, the mean arterial pressure remained elevated even with this longer collection time.

To continuously monitor the microvascular effects and avoid signal interference, 1-second *h*-NIRS and DCS measurements of the brain/skeletal muscle were recorded successively, with a full cycle occurred within 3.3sec. The use of two spectrometers allowed for *h*-NIRS measurements in the brain and in the skeletal muscle to be recorded simultaneously. Based on the time course data presented by Mawdsley (2021), we determined that a collection length of one second would be sufficient to detect the peak response. An additional benefit of acquiring *h*-NIRS and DCS simultaneously is the ability to measure scattering and dynamic absorption coefficients to improve the accuracy of DCS measures.

Furthermore, global tissue blood flow has been shown to increase with phenylephrine administration, but there is evidence that microvascular blood flow in some tissues decreases as a result (Maier, 2009). This is supported by skeletal muscle data; the total hemoglobin and flow decreased immediately post-bolus. However, they both increased to near baseline levels within the measurement window. This again suggests that there may be a brief period of blood flow redistribution. Future work will include incorporating intravital video microscopy into the methodology to conclusively determine if there is redistribution of flow in skeletal muscle after a phenylephrine bolus. Further, comparing results from non-invasive optical methods such as *h*-NIRS and DCS to invasive results obtained from intravital video microscopy would provide further insight into the response of the skeletal muscle and brain microvasculature.

2.5 References

1. Ellis, C.G., Jagger, J. and Sharpe, M.D., "The microcirculation as a functional system," Crit Care 9 Suppl 4, S3-S8 (2005).
2. Segal, S.S., "Regulation of blood flow in the microcirculation," Microcirculation 12(1), 33-45 (2005).
3. Ertmer, C., Morelli, A. and Westphal, M., "The role of phenylephrine in perioperative medicine," Yearbook of Intensive Care and Emergency Medicine 1, 483-491 (2009).
4. Dancker, C., Hopster, K., Rohn, K. and Kästner, S. B., "Effects of dobutamine, dopamine, phenylephrine and noradrenaline on systemic haemodynamics and intestinal perfusion in isoflurane anaesthetised horses," Equine Veterinary Journal 50(1), 104-110 (2018).
5. Van Leishout, J. J. and Secher, N. H., "Point:Counterpoint: Sympathetic activity does/does not influence cerebral blood flow," J Appl Physiol 105(4), 1364-1366 (2008).
6. Meng, L., Cannesson, M., Alexander, B. S., Yu, Z., Kain, Z. N., Cerussi, A. E., Tromberg, B. J. and Mantulin, W. W., "Effect of phenylephrine and ephedrine bolus treatment on cerebral oxygenation in anaesthetized patients," Br J Anaesth 107(2), 209-217 (2011).
7. Strandgaard, S. and Sigurdsson, S.T., "Counterpoint: Sympathetic activity does/does not influence cerebral blood flow," J Appl Physiol 105(4), 1366-1367 (2008).
8. Maier, S., Hasibeder, W. R., Hengl, C., Pajk, W., Schwarz, B., Margreiter, J., Ulmer, H., Engl, J. and Knotzer, H., "Effects of phenylephrine on the sublingual microcirculation during cardiopulmonary bypass," Br J Anaesth 102(4), 485-491 (2009).
9. Poterman, M., Vos, J. J., Vereecke, H. E. M., Struys, M. M. R. F., Vanoverschelde, H., Scheeren, T. W. L. and Kalmar, A. F., "Differential effects of phenylephrine and norepinephrine on peripheral tissue oxygenation during general anaesthesia: a randomized control trial," Eur J Anaesth 32(8), 571-580 (2015).
10. Hengstmann, J. H. and Goronzy, J., "Pharmacokinetics of ^{3}H-phenylephrine in man," European Journal of Clinical Pharmacology 21, 335-341 (1982).

11. Faraci, F. M. and Heistad, D. D., “Regulation of large cerebral arteries and cerebral microvascular pressure,” Circ Res 66(1), 8-17 (1990).
12. Hudlicka, O., “Microcirculation in skeletal muscle,” Muscles Ligaments Tendons J 1(1), 3-11 (2011).
13. Ogoh, S., Sato, K., Fisher, J. P., Seifert, T., Overgaard, M. and Secher, N. H., “The effect of phenylephrine on arterial and venous cerebral blood flow in healthy subjects,” Clin Physiol Funct Imaging 31(6), 445-451 (2011).
14. Paulson, O.B., Strandgaard, S. and Edvinsson, L., “Cerebral Autoregulation,” Cerebrovasc Brain Metab Rev 2(2), 161-192 (1990).
15. Christensen, L. K., Armstead, V.E., Bilyeu, D. P., Johnson, K. E. and Friesen, R.H., “Hemodynamic responses and plasma phenylephrine concentrations associated with intranasal phenylephrine in children,” Paediatr Anaesth 27(7), 768-773 (2017).
16. Boas, D. A. and Franceschini, M. A., “Haemoglobin oxygen saturation as a biomarker: the problem and a solution,” Philos Trans A Math Phys Eng Sci 369(1955), 4407-4424 (2011).
17. Durduran, T. and Yodh, A.G., “Diffuse correlation spectroscopy for non-invasive, microvascular cerebral blood flow measurement,” Neuroimage 85(1), 51-63 (2014).
18. Rajaram, A., Yip, L. C. M., Milej, D., Suwalski, M., Kewin, M., Lo, M., Carson, J. J. L., Han, V., Bhattacharya, S., Diop, M., de Ribaupierre, S. and St. Lawrence, K., “Perfusion and metabolic neuromonitoring during ventricular taps in infants with post-hemorrhagic ventricular dilation,” Brain Sci 10(7), 452 (2020).
19. Rajaram, A., Milej, D., Suwalski, M., Yip, L. C. M., Guo, L. R., Chu, M. W. A., Chui, J., Diop, M., Murkin, J. M. and St. Lawrence, K., “Optical monitoring of cerebral perfusion and metabolism in adults during cardiac surgery with cardiopulmonary bypass,” Biomedical Optics Express 11(10), 5967-5981 (2020).
20. Rajaram, A., Bale, G., Kewin, M., Morrison, L. B., Tachtsidis, I., St. Lawrence, K. and Diop, M., “Simultaneous monitoring of cerebral perfusion and cytochrome c oxidase by combining broadband near-infrared spectroscopy and diffuse correlation spectroscopy,” Biomedical Optics Express 9(6), 2588-2603 (2018).
21. Yeh, S.Y., “Comparative anorectic effects of metaraminol and phenylephrine in rats,” Physiol Behav 68(1-2), 227-234 (1999).

22. Diop, M., Wright, E., Toronov, V., Lee, T. and St. Lawrence, K., “Improved light collection and wavelet de-noising enable quantification of cerebral blood flow and oxygen metabolism by a low-cost, off-the-shelf spectrometer” J of Biomedical Optics 19(5), 057007 (2014).
23. Diop, M., Kishimoto, J., Toronov, V., Lee, D. C. S. and St. Lawrence, K., “Development of a combined broadband near-infrared and diffusion correlation system for monitoring cerebral blood flow and oxidative metabolism in preterm infants,” Biomedical Optics Express 6(10), 3907-3918 (2015).
24. Fantini, S., Franceschini, M.A. and Gratton, E., “Semi-infinite-geometry boundary problem for light migration in highly scattering media: a frequency-domain study in the diffusion approximation,” J. Opt Soc Am B 11(10), 2128 (1994).
25. Diop, M., Verdecchia, K., Lee, T. and St. Lawrence, K., “Calibration of diffuse correlation spectroscopy with a time-resolved near-infrared technique to yield absolute cerebral blood flow measurements,” Biomedical Optics Express 2(7), 2068-2081 (2011).
26. MATLAB. (2016). Version 9.1.0.441655 (R_2016b). Natick, Massachusetts: The MathWorksInc.
27. Thiele, R., Memergut, E. and Lynch, C., “The clinical implications of isolated alpha$_1$ adrenergic stimulation,” Anesthesia & Analgesia 113(2), 297-304 (2011).
28. Pires, P.W., Ramos, C.M.D., Matin, N. and Dorrance, A.M., “The effects of hypertension on the cerebral microcirculation”, Am J Physiol Heart Circ Physiol 304(12), H1598-H1614 (2013).
29. Shekar, S., Liu, R., Travis, O.K., Roman, R.J. and Fan, F., “Cerebral autoregulation in hypertension and ischemic stroke: a mini review”, J Pharm Sci Exp Pharmacol (1), 21-27 (2017).
30. Mawdsley, L. et al., “Using hyperspectral near infrared spectroscopy and diffuse correlation spectroscopy to monitor the microvascular effects of phenylephrine in vivo," Proc. SPIE 11639, Optical Tomography and Spectroscopy of Tissue XIV, 116390Z (2021).

Chapter 3

3 Conclusions

In this work we introduced a hybrid *h*-NIRS/DCS system that can continuously monitor the cerebral and skeletal muscle microcirculation to allow for the non-invasive measurement of tissue hemoglobin concentration and blood flow. Using this technology, the effect of phenylephrine across both microvascular beds was determined. Both the MAP response and the skeletal muscle response were expected; as MAP increased, blood flow and HbT in skeletal muscle decreased. However, HbT in the brain and CBF did not follow this same pattern, likely due to autoregulation.

Cerebral autoregulation disturbances are important to assess and control, especially in clinical settings (Durduran, 2014). As the brain has no way to store oxygen and any disruption in blood flow would quickly result in tissue oxygenation depletion (Boas, 2011). Further, cerebral autoregulation can be impaired by phenylephrine, which makes studying its effects on the brain microvasculature all the more important. The phenylephrine bolus caused an increase in systemic blood pressure but did not cause a consistent response in the brain. When the baseline MAP was lower than 95mmHg, blood flow and HbT increased in the brain. In contrast, when the baseline MAP was higher than 95mmHg, blood flow and HbT decreased. These findings suggest that CAR works to increase flow to the brain at baseline pressures lower than 95 mmHg, but decrease flow at pressures higher than 95mmHg. Since blood pressures above this point don't cause CAR to increase flow, the decrease seen may be due to the effects of phenylephrine on the large cerebral arterioles similar to what is seen in the muscle.

A benefit of near-simultaneous recording at two microvascular beds is that the response of each organ to same bolus can be compared. Phenylephrine causes vasoconstriction in arterioles in skeletal muscle, which is the driving force of the increase in MAP. The response in the brain is in direct contrast to the muscle, which has no stringent protective effect like CAR to keep flow at a certain level. The regularity of the MAP and the skeletal muscle flow response is consistent with skeletal muscle being the driving force of the MAP

increase, as muscle contraction and pressure are stable. Higher blood pressures seen in hypertension are associated with structural changes and dysfunctions that induce impaired cerebral autoregulation (Pires, 2013), (Shekar, 2017). This impairment is reflected in the results of the current work, where the response at higher blood pressures more closely mimics the response in skeletal muscle.

One limitation of this study is the near-simultaneous nature of the data collection. To continuously monitor the microvascular effects and avoid signal interference, 1-second *h*-NIRS and DCS measurements of the brain/skeletal muscle were recorded successively. To avoid cross-talk between systems, the *h*-NIRS subsystem could not be collecting at the same time as the DCS, and therefore the acquisition was not truly simultaneous. Data were collected in 1-second intervals with a total cycle time of 3.3s, which was the closest to simultaneous acquisition possible without impairing the integrity of the collected data. Based on the time course data presented by Mawdsley et al (2021), we determined that a collection length of one second would be sufficient to detect the peak response.

An additional benefit of acquiring *h*-NIRS and DCS simultaneously is the ability to capture scattering and dynamic absorption coefficients to improve the accuracy of DCS measures. However, this does bring forth a limitation - the estimated scattering coefficient from *h*-NIRS is lower than what is obtained from time-resolved NIRS. This potentially affects the accuracy of the DCS results. Due to the proportional nature of the absorption and the scattering coefficient, the lower estimated scattering coefficient means the absorption would be higher than expected. Changes in CBF are calculated instead of absolute values, meaning the absolute value of the scattering and absorption coefficients aren’t important. We accounted for the changes in these coefficients by incorporating the change in the absorption coefficient into the DCS analysis.

While this work is important in determining microvascular blood flow patterns in small animals, this specific set-up cannot be easily pivoted to adult humans. Both NIRS and DCS have been successfully used in clinical work, mainly in neonates for CBF measurements or skeletal muscle for children and adults. Due to the thickness of the adult human skull, a

more advanced data analysis that account for the skull contribution will be needed to obtain reliable cerebral measures in adult. Additionally, regional CBF measurements could be needed, which would require multiple source-detector pair. Given the small size of the adolescent rodent brain, it is reasonable to assume that flow to the majority of the brain tissue was measured in this work.

Global tissue blood flow has been shown to increase with phenylephrine administration, but there is evidence that microvascular blood flow in some tissues decreases as a result (Maier, 2009). This is supported by the data shown for skeletal muscle as the average response in total hemoglobin and in flow decreased immediately post-bolus. However, they both increased to near baseline levels within the collection window. This again suggests that there may be a brief period of blood flow redistribution. Future work will include incorporating intravital video microscopy into the methodology to conclusively determine if there is a redistribution of flow in skeletal muscle after a phenylephrine bolus. Further, comparing results from non-invasive optical methods such as *h*-NIRS and DCS to invasive results obtained from intravital video microscopy could provide new insight into the response of the skeletal muscle and brain microvasculature to phenylephrine.

Using this hybrid device in conjunction with intravital video microscopy will aid in determining disease progression in animal models. Many diseases have been shown to exhibit microvascular dysfunction before the onset of any clinical symptoms, such as sepsis and diabetes (Stehouwer, 2018), (Cade, 2008), (Ellis, 2005). A well-established sepsis model (Bateman, 2015) results in a 4-6 hours sepsis progression from initiation to end-point, and through intravital video microscopy the decline of microvascular health is clear. Adding *h*-NIRS and DCS to this protocol would provide another measure of skeletal muscle health, and more importantly a measure of cerebral health and the state of CAR during each stage of sepsis. Since the *h*-NIRS/DCS system is non-invasive, it could be used in both animal models and clinical studies which would aid in clinical translation of findings in animal models to bedside treatment.

This hybrid *h*-NIRS/DCS system is valuable for continuous *in vivo* monitoring (Rajaram, 2020a), (Rajaram, 2020b), and provides a unique method for concurrent monitoring of hemodynamic parameters. Using *h*-NIRS and DCS simultaneously to directly and continuously monitor hemodynamics in the brain and skeletal muscle microcirculation during a phenylephrine injection provided new insight into the timing and impact of vasoconstriction on major microvasculature beds, and the effect of cerebral autoregulation on external factors. The technology used here can be successfully integrated into a variety of drug and disease-based experiments to gain a clearer picture of the functioning of the microcirculation.

3.1 References

1. Durduran, T. and Yodh, A.G., “Diffuse correlation spectroscopy for non-invasive, microvascular cerebral blood flow measurement,” Neuroimage 85(1), 51-63 (2014).
2. Boas, D. A. and Franceschini, M. A., “Haemoglobin oxygen saturation as a biomarker: the problem and a solution,” Philos Trans A Math Phys Eng Sci 369(1955), 4407-4424 (2011).
3. Pires, P.W., Ramos, C.M.D., Matin, N. and Dorrance, A.M., “The effects of hypertension on the cerebral microcirculation”, Am J Physiol Heart Circ Physiol 304(12), H1598-H1614 (2013).
4. Shekar, S., Liu, R., Travis, O.K., Roman, R.J. and Fan, F., “Cerebral autoregulation in hypertension and ischemic stroke: a mini review”, J Pharm Sci Exp Pharmacol (1), 21-27 (2017).
5. Mawdsley, L. et al., “Using hyperspectral near infrared spectroscopy and diffuse correlation spectroscopy to monitor the microvascular effects of phenylephrine in vivo,” Proceedings Volume 11639, Optical Tomography and Spectroscopy of Tissue XIV, 116390Z (2021).
6. Stehouwer, C.D.A., “Microvascular dysfunction and hyperglycemia: a vicious cycle with widespread consequences,” Diabetes 67(9), 1729-1741 (2018).
7. Cade, W.T., “Diabetes-related microvascular and macrovascular diseases in the physical therapy setting,” Phys Ther 88(11), 1322-1335 (2008).
8. Ellis, C.G., Jagger, J. and Sharpe, M., “The microcirculation as a functional system,” Crit Care 9(Suppl 4), S3-S8 (2005).
9. Bateman, R. et al., “Sepsis impairs microvascular autoregulation and delays capillary response within hypoxic capillaries,” Crit Care 19, 389 (2015).
10. Rajaram, A., Yip, L. C. M., Milej, D., Suwalski, M., Kewin, M., Lo, M., Carson, J. J. L., Han, V., Bhattacharya, S., Diop, M., de Ribaupierre, S. and St. Lawrence, K., “Perfusion and metabolic neuromonitoring during ventricular taps in infants with post-hemorrhagic ventricular dilation,” Brain Sci 10(7), 452 (2020a).
11. Rajaram, A., Milej, D., Suwalski, M., Yip, L. C. M., Guo, L. R., Chu, M. W. A., Chui, J., Diop, M., Murkin, J. M. and St. Lawrence, K., “Optical monitoring of cerebral

perfusion and metabolism in adults during cardiac surgery with cardiopulmonary bypass,” Biomedical Optics Express 11(10), 5967-5981 (2020b).

Curriculum Vitae

Education:

BScH in Life Sciences
Queen's University
Kingston, Ontario, Canada
2012-2018

MSc in Medical Biophysics
The University of Western Ontario
London, Ontario, Canada
2018-2021

Honours and Awards:

Travel Award
Microcirculatory Society for Experimental Biology
2020 | $495USD

Trainee of the Month
Biomedical Imaging Research Centre
2020

Best Trainee Presentation
Canadian Critical Care Trials Group
2019

Travel Award
Canadian Critical Care Trials Group
2019 | $500 CAD

Western Graduate Research Scholarship
Western University
2018-2020 | $4500 CAD/year

Dean's List
Queen's University
2016-2018

Presentations and Talks

Poster Presentation (Virtual)
Experimental Biology
April 2021

Invited Conference Presentation (Virtual)
SPIE Photonics West
March 2021

Seminar Talk
Medical Biophysics Seminar Series
March, October 2020

Trainee Presentation
Canadian Critical Care Trials Group
June 2019

Poster Presentation
London Health Research Day
May 2019

Publications:

Mawdsley, L., Rajaram, A., Yip, L.C.M., Abayomi, N., Milkovich, S., St. Lawrence, K., Carson, J.J.L., Ellis, C.G. and Diop, M., "Using hyperspectral near infrared spectroscopy and diffuse correlation spectroscopy to monitor the microvascular effects of phenylephrine in vivo," Proc. SPIE 11639, Optical Tomography and Spectroscopy of Tissue XIV, 116390Z (2021).

Mendelson, A. et al., "National preclinical sepsis platform: developing a framework for accelerating innovation in Canadian sepsis research," ICMx 9, 14 (2021). [22nd author]

In review:

Christie, J., Kong, I., **Mawdsley, L**., Milkovich, S., Doornekamp, A., Baek, J., Fraser, G.M., Ellis, C.G. and Sove, R., "Optical method to determine in-vivo capillary hematocrit, hemoglobin concentration, and 3-D network geometry in skeletal muscle,".

Conference abstracts:

Mawdsley, L., Rajaram, A., Yip, L.C.M., Abayomi, N., Li, N., Milkovich, S., St. Lawrence, K., Carson, J.J.L., Ellis, C.G. and Diop, M., "Simultaneous monitoring of the cerebral and skeletomuscular microcirculation using hyperspectral near infrared spectroscopy and intravital video microscopy," FASEB Journal 35(S1) (2021).

Mawdsley, L., Rajaram, A., Yip, L.C.M., Ellis, C.G. and Diop, M., "Using near infrared spectroscopy, diffuse correlation spectroscopy, and intravital video microscopy to monitor the skeletomuscular and cerebral microcirculation," FASEB Journal 34(S1) (2020).